MIR-143 ACTIVATION REGULATES SMOOTH MUSCLE AND ENDOTHELIAL CELL CROSSTALK IN PULMONARY ARTERIAL HYPERTENSION

Lin Deng*[1], Francisco J. Blanco*[1], Hannah Stevens[1] Ruifang Lu[1#], Axelle Caudrillier[1], Martin McBride[1], John D McClure[1], Jenny Grant[1], Matthew Thomas[2#], Maria Frid[3], Kurt Stenmark[3], Kevin White[1$,] Anita G. Seto[4], Nicholas W. Morrell[5], Angela C Bradshaw[1], Margaret R. MacLean[1], Andrew H. Baker[1]

[1]Institute of Cardiovascular and Medical Sciences, University of Glasgow, Glasgow, G12 8TA, UK.
[2]Novartis Institutes for BioMedical Research Horsham UK.
[3]Division of Critical Care Medicine/Cardiovascular Pulmonary Research Laboratories, Department of Pediatrics and Medicine, University of Colorado Denver, Aurora, CO 80045, USA.
[4]MiRagen Therapeutics, Inc, Boulder, CO.
[5]Division of Respiratory Medicine, Department of Medicine, Addenbrooke's Hospital, University of Cambridge School of Clinical Medicine, Cambridge, CB2 0QQ, UK.
#Present address: King's British Heart Foundation Centre, King's College London, 125 Coldharbour Lane, London SE59NU, United Kingdom.
#Present Address, AstraZeneca R&D Mölndal, R&D | Respiratory, Inflammation and Autoimmunity (RIA) Innovative Medicines, Building AC461, SE-431 83 Mölndal, Sweden
$Present Address, Novartis Institutes for BioMedical Research, Inc.,250 Massachusetts Avenue, Cambridge, MA 02139, United States.

*These authors contributed equally.

Corresponding author: Prof. Andrew H. Baker
Institute of Cardiovascular and Medical Sciences
University of Glasgow
Glasgow, G12 8TA, UK.
Tel No: +44 0141 330 1977
Fax No: +44 0141 330 3360
E-mail: Andrew.H.Baker@glasgow.ac.uk

Running title: Regulation and role of miR-143 in PAH

Subject codes:
[143] Gene regulation
[89] Genetics of cardiovascular disease
[130] Animal models of human disease
[18] Pulmonary circulation and disease
[14] Other hypertension

ABSTRACT

Rationale. The pathogenesis of PAH remains unclear. The four microRNAs representing the miR-143 and miR-145 stem loops are genomically clustered.

Objective. To elucidate the transcriptional regulation of the miR-143/145 cluster, and the role of miR-143 in PAH.

Methods and Results. We identified the promoter region that regulates miR-143/145 miRNA expression in pulmonary artery smooth muscle cells (PASMCs). Using a reporter vector, we characterized and mapped PAH-related signaling pathways, including estrogens receptor (ER), liver X factor/retinoic X receptor (LXR/RXR), TGF-β (Smads), and hypoxia (HRE) that regulated levels of all pri-miR stem loop transcription and resulting miRNA expression. We observed that miR-143-3p is selectively upregulated compared to miR-143-5p during PASMC migration. Modulation of miR-143 in PASMCs significantly altered cell migration and apoptosis. In addition, we found high abundance of miR-143-3p in PASMCs-derived exosomes. Using assays with pulmonary arterial endothelial cells (PAECs) we demonstrated a paracrine pro-migratory and pro-angiogenic effect of miR-143-3p enriched exosomes from PASMC. Quantitative PCR and in situ hybridisation showed elevated expression of miR-143 in calf models of PAH as well as in samples from PAH patients. Moreover, a protective role for miR-143 in experimental PH in vivo was demonstrated in miR-143-/- and antimiR143-3p-treated mice exposed to chronic hypoxia in both preventative and reversal settings.

Conclusions. MiR-143-3p modulated both cellular and exosome-mediated responses in pulmonary vascular cells, whilst inhibition of miR-143-3p blocked experimental PH. Taken together these findings confirm an important role for the miR-143/145 cluster in PAH pathobiology.

Key Words: microRNA, pulmonary hypertension, exosomes, transcriptional regulation, cell migration

Non-standard Abbreviations and Acronyms.

9cRA: 9-*cis*-Retinoic acid
22R: 22R-Hydroxycholesterol
BMP: Bone morphogenetic protein
ER: Estrogen receptor
HPAH: heritable PAH
HRE: Hypoxia response element
IPAH: idiopathic PAH
LXR/RXR: Liver X Receptor/Retinoic X Receptor
miRNAs: Non-coding microRNAs
PAECs: Pulmonary artery endothelial cells
PAH: Pulmonary arterial hypertension
PASMCs: Pulmonary artery smooth muscle cells
PCNA: Proliferating Cell Nuclear Antigen
PDGF: Platelet-Derived Growth Factor
PH: Pulmonary hypertension
qPCR: Quantitative PCR
RV: Right ventricle
RVH: Right ventricular hypertrophy
RVP: Right ventricular pressure
SAP: Systemic arterial pressure
TGF-β: Transforming growth factor-β
TF: Transcription factors
TSS: Transcription start site
VEGF: Vascular Endothelial Growth Factor

INTRODUCTION

Pulmonary arterial hypertension (PAH) is a rare, severe and progressive disease with an estimated prevalence of ~15 cases per million[1]. The pathogenesis of PAH includes sustained vasoconstriction and abnormal progressive fixed vascular remodelling. This is accompanied by endothelial dysfunction and activation of fibroblasts and smooth muscle cells[2]. PAH may be initiated by loss of endothelial integrity and dysfunction resulting in exposure of underlying cells to circulating factors, leading to proliferation and apoptosis resistance in the adventitia, smooth muscle media and the formation of a neointima[3]. Clinically, PAH is subdivided into several groups, including: idiopathic (IPAH), heritable (HPAH) and PAH associated with other diseases (APAH). Female gender is considered a risk factor *per se* for all PAH subtypes, since it is more frequent in women than men[4].

Most cases of HPAH (>70%), and some IPAH cases (approximately 20%), are caused by mutations in the bone morphogenetic protein type II receptor gene (*BMPR2*) that impairs BMP signaling pathway via Smad1, Smad5 and Smad8, and leads to an increased activity of TGF-β pathway via non-canonical and canonical Smad2/3 signalling[5]. However, since PAH is incompletely penetrant, *BMPR2* mutations alone may not be sufficient to cause disease, so that a 'second hit' including other genetic and/or environmental factors may be required for the clinical manifestation of PAH[6]. Triggers for disease may include inflammation, hypoxia and shear stress or vascular injury.

MicroRNAs (miRNAs) are small non-coding RNAs that negatively regulate gene expression by recognizing the 3'-untranslated regions (3'-UTR) of target coding mRNAs and abolishing their expression by blocking translation or accelerating their degradation[7]. Coding sequences of miRNA are distributed across the entire genome and can be classified by their location in either intragenic, typically within an intron sequence (mirtrons), or intergenic regions. An independent promoter region drives expression of intergenic miRNAs. Thus, most intergenic miRNAs are transcribed by RNA polymerase II and the basal transcriptional machinery[8]. Although little is known about the transcriptional regulation of miRNA expression, this process has been proposed to be orchestrated by the cellular pool of transcription factors that interact with the promoter region similarly to protein coding genes. Recent studies have developed bioinformatics algorithms to predict the miRNA core promoters, focused on the upstream sequence of the precursor (pri-miRNA)[9]. In the particular case of intergenic miRNA, the promoter region is predicted to be ~20 kb upstream of the pri-miRNA and exhibits similar conservation patterns to the promoters of protein coding genes. Nonetheless, only a few papers have reported experimental evidence that validate those regions as core promoters.

In blood vessels, one of the most studied miRNA expressed by vascular smooth muscle cells (VSMC) is the miR-143/145 cluster, which has a pivotal role in VSMC differentiation and disease[10-12]. MiR-145 expression has been reported to control VSMC phenotype, restoring the contractile phenotype in atherosclerotic plaques[13] and coronary collateral growth in the metabolic syndrome[14], among others. Expression of the miR-143/145 cluster is decreased in conditions associated with acute and chronic vascular stress, such as aortic aneurysms[12] and coronary artery disease[15]. MiR-145-5p is able to control vascular neointimal lesion formation[16]. Up-regulation of miR-145-5p was observed in pulmonary artery VSMCs and in lung tissue from patients with idiopathic and heritable pulmonary arterial hypertension (PAH)[17]. However, the transcriptional regulation of the cluster has not been defined with respect to mediators of PAH nor has the role of miR-143 been addressed in PAH. Interestingly, despite their predominantly intracellular localization, miRNAs have been recently found in extracellular compartments, such as exosomes[18]. These exosomes represent a specific subtype of secreted membrance vesicles of 30-130 nm formed through the fusion of multivesicular endosomes with the

plasma membrane[19]. Exosomes convey a wide array of molecules such as proteins and nucleic acids, including mRNAs and miRNAs, and have emerged as regulators of cell-cell communication and paracrine signaling mediators during physiological and pathological processes in various diseases[20, 21]. Here, we studied the transcriptional regulation of the miR-143/145 cluster and its contribution to the development of PAH.

METHODS

Cell culture methods and reagents[17]; cloning the miR-143/145 proximal promoter and reporter vectors analysis RNA extraction, reverse transcription and TaqMan qPCR Analysis[17] and *in situ* hybridisation; Smad3 decoy assays; Isolation of exosomes from cell media; Cell migration[22] and proliferation[23] assays; Western blot and immunohistochemistry analyses[24]; Animal housing and experimentation including chronic hypoxia exposure and hemodynamic measurements[24]; and Statistical analysis, were carried out as previously reported elsewhere and are described in the expanded Methods section in the online data supplement, available online at http://circres.ahajournals.org.

RESULTS

Identification and cloning of the MIR143HG promoter

We first sought to define the transcriptional regulation of the miR-143/145 cluster. According to miRStart data and using the human genome assembly GRCh38, the transcription start site (TSS, position +1) is likely to be located at position 149406877 in the plus strand of chromosome 5, 22,041 bp upstream of the pri-miR143 precursor. Supporting this TSS, we identified a local TATA-box at position (-26) (TATAAG), as well as 2 likely CAAT-boxes (CCAAT) at positions (-94) and (-54), and an E-box at position (-113) (CACGTG) (Figure 1A).

We selected a GC-rich (58.5%) region of 1.5 kb spanning from position (-1354) to (+202), since the alignment with the homologous region from other mammalian species was strong (match >60%). A proximal region of 0.5 kb was also selected from (-304) to (+202) for mapping transcriptional activity. Despite some GC-rich regions in the promoter, no putative CpG islands were predicted and experimentally the DNA demethylating reagent 5-Aza-2'-deoxycytidine did not affect the pri-miR-143/145 expression either in PASMC or PAEC/HUVEC (Supplementary Figure S1).

Analysis of TF binding sites

The *in silico* analysis of the 1.5kb sequence of miR-143/145 promoter revealed a number of putative binding sites for transcriptional factors (TFs). We treated PASMC with their respective ligands, and pri-miR precursors and mature forms were detected by qPCR and luciferase reporter assays. Based on 3 predicted estrogen receptor binding sites at position (-1129), (-801) and (-14), we treated PASMC with estradiol (E2). E2 induced the expression of both pri-miR-143 and pri-miR-145 after 24 h (Figure 1B). The respective mature lead strand miRNAs were upregulated correspondingly (Figure 1C). Reporter vectors confirmed the increased transcriptional activation of the miR-143/145 promoter in response to E2 (Figure 1D). Using site-directed mutagenesis, we studied which of the 3 ER sites are necessary for ER-dependent induction of miR-143. We identified that the sites at positions (-801) and (-14) are required since the activity of the promoter is not enhanced when these sites are mutated.(Figure

1E). We also identified several putative binding sites for the retinoic acid receptor, which is well known to act in combination with the liver X receptor (LXR/RXR)[25]. PASMC treated with 9-*cis*-retinoic acid (9cRA) and/or 22R-hydroxycholesterol (22R) upregulated both precursor and mature forms of the cluster (Figure 1F and 1G). The transcriptional activity of the reporter vectors showed a small but significant induction for the minimal promoter (p0.5-luc) but this was more marked for the full-length sequence (p1.5-luc) (Figure 1H). Activity was dependent on the binding sites located at (-673), (-4) and (+98) (Figure 1I). We also identified 2 putative hypoxia response elements (HRE) and, upon stimulation, we observed a 2-fold induction in pri-miR-143 expression and moderate induction for pri-miR-145 in PASMC cultured in hypoxic conditions (Figure 1J). Expression of mature miR-143-5p and -3p were upregulated in the same pattern but only miR-145-5p and not miR-145-3p was induced (Figure 1K). Moreover, both minimal and full-length reporters responded to hypoxia (Figure 1L). Mutation analysis confirmed that the HRE site in (-113) which overlaps the basal transcription element E-box, was critical since the minimal promoter p0.5-luc maintains the response to hypoxia (Figure 1M). We also searched for STAT sites in the MIR143HG promoter. It was predicted *in silico* that several consensus sites for STAT5A, STAT5B, STAT1 and STAT3 were in the region between (-1354) and (-304). None were located in the minimal 0.5kb region.

The miR-143/145 promoter responds to TGF-β

Several putative binding sites for Smad proteins for both TGF-β and BMPs signaling pathways were localised (Figure 1A). TGF-β1 increased the expression of precursor and the 4 mature forms of the miR-143/145 cluster (Figures 2A and 2B) in PASMC. Moreover, treatment of cells with a specific inhibitor of the TGF-β receptor ALK5, SB525334, completely abolished this induction (Supplementary Figure S2). In contrast, BMP4 treatment did not affect the basal levels of the precursor forms or the mature miRNAs (Figure 2A and 2B). We therefore focused on 2 putative Smad3 binding sites. Because TGF-β1 induced the transcriptional activity of the full length reporter but not the minimal p0.5-luc construction (Figure 2C), we assayed the Smad3 element at position (-592). Site-directed mutagenesis of this Smad3 binding site abolished the activity of the reporter in response to TGF-β1 (Figure 2D). Next, using release 138 of the 1000 Genomes Project[26] on Ensembl we found 3 single nucleotide polymorphisms (SNPs) affecting the Smad3 binding site at position (-592). One of these was outside the consensus motif (rs145177914, [C>T]). However, the remaining two disrupted the Smad3 binding site (rs12517403, [T>C]; and rs116423755, [G>A]). To test the functionality of this, a Smad3 decoy assay was designed using FAM-labelled PTO-ODN bearing the SNPs. The wild type and a scramble sequence were used as controls. A dose-response assay co-transfecting WT and mock probes in PASMC, with or without TGF-β1 treatment, demonstrated that increasing WT probe reduces the expression of pri-miR-143 and pri-miR-145, as well as Col1A1 as a TGF-β1 positive control, validating this sequence as a Smad3 binding site (Supplementary Figure S3). Furthermore, PTO-ODN probes bearing Smad3 SNPs were unable to block the TGF-β1 stimulus, confirming the functionality of that Smad3 site (Figure 2E and 2F).

Manipulation of miR-143/145 cluster affects PASMCs migration

We sought to assess the impact of promoter activation on PASMC migration, proliferation and apoptosis. We first sought to assess the effect of wound assay on induction of the miR-143/145 axis in response to this stress and during the healing response. Using wounding assays, we showed rapid transcriptional activation of the pri-miR-143/145 precursors at 3 h, which was maintained over time for pri-miR-143 but later repressed for pri-miR-145 (Figure 3A). Pri-miR-143 up-regulation was accompanied by a corresponding increase in mature miR-143-3p. By contrast, miR-145-5p expression

did not change during cell migration (Figures 3B). In addition, the expression of their respective passenger strands, miR-143-5p and miR-145-3p, did not change significantly during the wound closure (Figure 3C). These responses were also observed but even enhanced in distal PASMC from PAH patients (Supplementary Figure S4). Moreover, overexpression of miR-143-3p using pre-miRNA significantly induced PASMCs migration, while antimiR-mediated knockdown of miR-143-3p decreased the migration rate (Figure 3D-G). In contrast, stimuli reduced cell migration and altered the expression pattern of pri-miR-143 and pri-miR-145 (Supplementary Figure S5). Q-PCR confirmed the overexpression and knockdown of miR-143 (Figure 3F and G). In contrast, using the BrdU incorporation assay and PCNA protein analysis, PASMC proliferation did not change in cells treated with pre-miR143 compared to the control groups whereas apoptosis was induced with antimiR-143 (Supplementary Figure S6A-C). We also assessed the influence of DNA damage to miR-143 expression in PASMC. We treated PASMC with TNF-α (100 ng/mL), IL-6 (100 μM) or PDGF (30 ng/mL) for 48 h to induce DNA damage. γH2AX nuclear staining confirmed DNA damage in PASMC and miR-143 expression was upregulated (See Supplementary Figure 6D, E). Further, we assessed the miR-143/145 promoter activity during cell migration. We analysed GFP reporter vectors from the promoter sequence by nucleofection in PASMC. Both minimal (0.5kb) and full-length (1.5kb) promoter constructions showed GFP induction in migrating cells leading from the scratch wound border (Figure 3H-J). We next performed a gene expression microarray experiment on PASMCs transfected with the miR-143 mimic and identified 68 regulated targets that are involved in cell migration (Table S1). Further, "migration of cancer cells" was identified as a significantly enriched pathway (p=0.0001) identified by ingenuity pathway analysis (Table S2 and Supplementary Figure S7). These findings are consistent with the hypothesis that miR-143 can increase migration in PASMCs. We did not observe an effect of miR-143 knockout on FAK in total lung homogenates (Supplementary Figure S8A,B). Potentially, Stat3 could have a role in the transcriptional regulation of miR-143. However, we observed no increase in STAT 3 (phospho Y705) by western blotting in migrating PASMCs, although miR-143 was upregulated 5 fold in these cells (Supplementary Figures S8C,D).

miR-143-3p induced in PASMCs can be transferred to PAECs and induces endothelial cell migration

Having observed increased levels of miR-143-3p in PASMC exposed to PAH stimuli, we explored whether miR-143-3p was involved in cell-cell communication between PASMCs and PAECs. We performed a co-culture assay of PAEC with PASMC in Boyden chambers, in which cells were physically separated by a membrane to prevent direct cell-cell contact (Figure 4A). In order to visualize whether miRNAs released from PASMCs in extracellular vesicles are transported to PAECs, we transfected PASMC with a Cy3-labeled precursor miRNA prior to co-culturing with PAECs for 24 h. Fluorescence imaging of PAECs showed that Cy3-labeled miRNAs derived from PASMCs could be detected in PAECs in the co-culture system (Figure 4B). Moreover, the basal level of miR-143-3p in PAECs was upregulated by co-culture with PASMC showing transfer of endogenous miR-143 (Figure 4C). Levels of miR-143 were upregulated after co-culture with miR-143-transfected PASMCs for 24 h and 48 h (Figure 4D). or PAECs co-cultured with miR-143-3p transfected PASMCs (Figure 4E, G) or exposed to conditioned medium from transfected PASMCs showed increased migration compared to controls (Figure 4G, H). Q-PCR confirmed the increase in miR-143-3p in recipient PAECs.

Extracellular miR-143-3p transport is mediated by exosomes

Previous studies have reported that exosomes can carry functional miRNAs between cells[18, 27]. To investigate the function of the extracellular vesicles containing miR-143-3p in the co-culture system

and condition medium, we isolated exosomes from the medium of PASMCs transfected with different concentrations of pre-miR143-3p and quantified the levels of miR-143-3p in the exosomes and transfected cells. MiR-143-3p expression was clearly detected by qPCR in PASMC-derived exosomes from culture supernatant, which displayed the expected diameter and size and markers (Figure 5A-C). The incorporation of miR-143-3p into exosomes was confirmed by qPCR assessing both the cell-associated and extracellular levels of miR-143-3p 24 h post-transfection. As expected, we found a dose-dependent increase in miR-143-3p in PASMCs (Figure 5D) and accumulation of miR-143-3p in exosomes derived from PASMCs (Figure 5E). In addition, we performed a wound-healing assay to examine whether exosome-derived miR-143-3p has similar functional effects on PAECs to that observed in the co-culture and conditioned medium experiments. PASMC-derived exosomes induced PAEC migration in a similar manner to that observed in co-culture and conditioned medium experiments (Figure 5F), with a corresponding increase in the intracellular levels of miR-143 (Figure 5G). This resembled the effect of direct transfection of the miR-143 precursor into PAECs (Figure 5H and 5I). Further, exosome-derived miR-143 or direct transfection of pre-miR-143 induced angiogenesis in matrigel assays in PAEC (Figure 5J-L). Direct transfection with pre-miR-143-3p in PAECs had no effect on cell proliferation analyzed by PCNA western blot and BrdU incorporation or apoptosis (Supplementary Figure S9A-D). Using a Cy3-labelled pre-miR-143 transfected into PASMC and purification of resulting PASMC-derived exosomes, we demonstrated uptake into PAEC by fluorescence microscopy (Supplementary Figure S9E). Finally, we demonstrated that the induction of migration by miR-143-enriched PASMC-derived exosomes in PAEC was inhibited by transfection of the PAEC by antimiR-143 (Supplementary Figure S9F, G). We also carried out an expression microarray on PAECs treated with exosomes from PASMCs transfected with scramble or pre-miR-143. We observed the regulation of multiple targets involved in cell death and survival (Table S3 and S4). Further these targets might suggest that miR-143 reduces cell death in PAEC (Supplementary Figure S10).

MiR-143-3p is upregulated in PAH *in vivo* in animals and in humans

The involvement of miR-143-3p in PAH has not been investigated. Based on the above data, we sought to address this using experimental models and human samples. We found a consistent up-regulation of miR-143-3p expression in whole mouse lung (Figure 6A) and right ventricle (Figure 6B) in response to hypoxia. Further, in primary PASMC from PAH patients, both miR-143-3p and -5p expression levels were also significantly upregulated compared to control PASMC from healthy volunteers (Figure 6C). *In situ* staining also highlighted the expression of miR-143-3p in the RV of mouse hearts showing elevation after hypoxia (Supplementary Figure S11A). Further, qPCR studies showed the presence of miR-143-5p and -3p in both cardiomyocyte and fibroblast cells derived from normal mouse hearts (Supplementary Figure S11B). Furthermore, *in situ* staining also revealed increased miR-143 in the vascular wall of the small pulmonary arterioles of hypoxic neonatal calves and cattle with Brisket disease, a naturally occurring large animal model of hypoxic pulmonary hypertension (Figure 6D and Supplementary Figure S12A). Early and sustained activation of miR-143 was observed in the rat sugen/hypoxia model (Supplemenatary Figure S12B). Correlating with these findings in PAH animal models, miR-143-3p expression was also increased in the smooth muscle layer of constrictive and complex arterial lesions of PAH patients compared with healthy controls (Figure 6E).

Direct knockout of miR-143 stem loop and pharmacological inhibition of miR-143-3p in mice alleviates the development of PH *in vivo*

Finally, we evaluated the effect of genetic ablation of the miR-143 stem loop on the development of PH. To test this, we challenged 8-week-old miR-143$^{-/-}$ mice (KO) and age-matched control mice with 14-day exposure to chronic hypoxia. Although miR-143 KO had no effect on systemic arterial pressure (SAP) (Figure 7A), there was a significant reduction in right ventricular systolic pressure (RVSP) and right ventricular hypertrophy (RVH) in miR-143 KO mice compared to wild-type controls (Figure 7B and 7C). MiR-143 has been shown to decrease Akt-Ser473 phosphorylation[28]. We did not observe a difference in AktSer473 phosphorylation in RV extracts from controls vs miR-143-/- mice (Supplementary Figure S13). Histopathologically, and consistent with the hemodynamic data, miR-143 KO mice exhibited a significant reduction in pulmonary vascular remodelling when compared with wild-type mice (Figure 7D).No effect was observed on microvascular density in the RV from KO mice vs controls (Supplementary Figure S14). The induction of migration and tube formation observed by exosomal miR-143 transfer might be beneficial in the context of microvessel perfusion. We assessed microvessel density in the lungs of hypoxic WT and miR-143-/- animals. We observed a significant reduction in the number of vessels in the lungs of miR-143-/- vs WT mouse lungs (Supplementary Figure 14E). To test whether knock-down of miR-143-3p could reverse experimental PH *in vivo*, synthetic anti-miRNA specific for miR-143-3p was subcutaneously delivered to mice exposed to chronic hypoxia on days 1 and 8 of the 14-day hypoxic exposure (Figure 7E). To verify down-regulation of miR-143, we measured miR-143-3p in treated mice by qPCR of RNA from whole lung homogenates or isolated pulmonary arteries (Supplementary Figure S15A-C). In normoxic conditions, RVSP and RVH were unchanged (Figure 7F and 7G). For the treated mice exposed to chronic hypoxia, the miR-143-3p anti-miRNA group showed a significant reduction in RVSP compared with vehicle- and scramble-treated groups (Figure 7F). By contrast, no changes were observed in RVH, systemic arterial pressure and vascular remodelling (Figure 7G and H, Figure S16). PCNA analysis demonstrated that miR-143 KO did not affect cell proliferation during hypoxia-induced PH model *in vivo*, consistent with in vitro cell proliferation results (Supplementary Figure S15 D,E). Finally, we performed a reversal study with induction of hypoxia prior to initiation of antimiR-143 treatment (Figure 7I-L). We show that delayed antimiR-143 treatment reverses RVSP, RVH and decreased vascular remodelling compared to controls (Figure S16).

DISCUSSION

In the current study, we identified the promoter region and characterized several PAH-related signaling pathways that regulate miR-143/145 expression. Moreover, we demonstrated novel miR-143-3p/exosome-mediated cell-cell communication between PASMCs and PAECs, contributing to the SMC and EC cell migratory phenotypes that are involved in the pathogenesis of PAH. In addition, *in vivo* data revealed genetic deletion and pharmacological inhibition of miR-143 prevented the development of hypoxia-induced PH and reversed it when given after the induction of hypoxia.

Our previous study demonstrated that elevated levels of miR-145-5p in the lung vasculature are associated with PAH. This scenario was further corroborated in a PH mouse model and using miR-145 knock-out mice, which exhibited a protective phenotype during the development of hypoxia-induced PH[17]. Coding sequences for miR-143 and miR-145 are highly conserved, and lie in close proximity to each other on murine chromosome 18 and human chromosome 5. However, the promoter region and the transcriptional regulation of miR-143/145 expression have hitherto been unknown, except for a previous paper reporting a serum response element ~3.3kb upstream from the pri-miR-143 locus[29].

Bioinformatics tools predicted the TSS for this miRNA cluster to be located about ~22 kb upstream of the pri-miR-143 precursor. Here, we have dissected some of the signaling pathways that regulate miR-143/145 expression at the promoter level. Firstly, the estrogen receptor clearly triggers the expression of the cluster, which is in line with the fact that gender *per se* is a risk factor for the development of PAH[30]. Our studies used female mice and it would be important to study equivalent strategies in males. We found 2 ER binding sites which seem to cooperate in effective stimulation. In the same way, up to 3 different LXR/RXR binding sites appear to cooperate in the response to 9cRA and oxysterols such as 22R. These oxysterols are oxidized species derived from cholesterol and it has been recently reported that their levels are increased in the vasculature of patients with hypoxic conditions[31]. Indeed, hypoxia itself can clearly induce the expression of the cluster. This is in keeping with the fact that approximately 20% of hypoxia-induced transcripts are for non-coding RNA[32], in line with the role of chronic hypoxia and reactive oxygen species in the development of pulmonary hypertension [33]. In addition, we assessed the impact of TGF-β signaling on this novel promoter region. In agreement with previous reports[5, 34], we demonstrate that TGF-β1, but not BMP4, induces the expression of miR-145 and miR-143. No further characterization was carried out previously regarding the Smad binding site(s) involved. Although we have identified an important component of the regulation of the miR-143/145 cluster in identification of a promoter region, our study provides limited knowledge relating to the regulation of the promoter by transcription factors in response to wound healing. Further studies will be required to address this limitation.

Cell proliferation and migration are both necessary for vascular remodeling, and their dysregulation in PAEC and PASMC compartments is associated with PAH pathophysiology, as numerous *in vivo* and *in vitro* studies have previously shown[10, 35, 36]. Recently, several studies have reported that miRNAs associated with vascular remodeling can regulate cell proliferation and migration (reviewed by Grant *et al*., 2013)[37]. Our previous study on miR-145 demonstrated that miR-145 mimic delivery inhibits cell proliferation of PASMCs, but had no effect on cell migration[17]. In addition, other studies have shown that miR-143 and miR-145 are not redundant and hence do not always act in parallel *in vitro* and *in vivo*[10, 29]. We found a sustained and significant up-regulation of both pri-miR-143 and mature miR-143 from 3 hours to 24 hours in migrating PASMCs, which was not mirrored by changes in miR-145. This suggests that there may be differential post-transcriptional regulation of each individual miRNA within the cluster. This alternative processing has been already reported for other miRNA clusters, for example the up-regulation of all members of the polycistronic miR-17~92 cluster during endothelial differentiation of mouse embryonic stem cells apart from miR-92a, which is repressed[38]. Nevertheless, even though the transcriptional up-regulation of pri-miR-143/145 occurs early, and the fact that the promoter sequence has putative binding sites for KLF6, a transcription factor recently related to vascular cell migration[22], we found that this pathway is not involved in PASMC migration. Here we demonstrate that miR-143-3p significantly increases during cell migration. We also show that miR-143 overexpression induces PASMC migration, whereas miR-143-3p knock-down inhibits this effect. This reduction in cell migration is consistent with *in vivo* data showing that miR-143 KO mice (and mice treated with antimiR) exhibit protection from PH. By contrast, we did not observe any effect of miR-143 on the proliferation of PASMCs *in vitro* or *in vivo*, as measured by PCNA expression and BrdU analysis. Consequently, the fact that miR-143 has been previously reported as a tumor suppressor by inhibiting proliferation and migration in several cancer cells[39, 40] suggests that its function strongly depends on the specific cellular context. Mechanistically, we used an unbiased approach to assess the effect of miR-143 mimic on the transcriptional profile of PAMSCs. Informatic analysis of the data highlighted a migratory phenotype. MiR-143 may act via multiple mechanisms in PASMCs and indeed PAEC following exosome-mediated transport and uptake, including cell migration and apoptosis (PASMC) and cell death/survival and angiogenesis (PAEC). This will require detailed

further analysis but suggests a complex environment where miR-143 upregualtion in hypoxia or inhibiton (therapeutically) can modulate phenotypes in both PASMC and PAEC compartments. A recent study has highlighted the importance of cell:cell transport from SMC to EC and resulting function of the miR-143/5 axis on angiogenesis through modulation of genes including hexokinase-2[41]. We did not observe equivalent changes in hexokinase-2 (not shown), perhaps reflecting differences in transport mechanisms observed and/or receipent cell types (here primary PAEC). Clearly, cell:cell communication of miR-143 (and likely miR-145) is of fundaemental importance in related pathological settings. As we observed both cardiac and lung phenotypes with miR-143 loss, the generation of conditional knockouts will help define cell-specific contributions to the underpinning role of miR-143 in this setting.

It was recently reported that exosomes are effective carriers of miRNAs, and the identification of exosomal miRNAs has been performed by a number of researchers[21]. Exosomes are known to be mediators of extracellular communication in cardiovascular diseases, including atherosclerosis[20], cardiac hypertrophy[42] and myocardial infarction[43]. Previous studies demonstrated that exosomes derived from endothelial cells convey both miR-143 and miR-145 to smooth muscle cells, affecting their vascular functions[20]. Therefore, it is reasonable to speculate that cell-cell communication in the pulmonary vascular system is relevant to the cellular function changes that participate in the pathogenesis of PAH. In the current study, we identified a novel exosome-mediated miRNA communication between PASMCs and PAECs, contributing to the induction of smooth muscle cell-stimulated endothelial cell migration. We provide the first evidence that miR-143 acts as a paracrine signalling mediator and is involved in the induction of PAEC migration but not proliferation. We found that isolated exosomes from PASMC culture medium are enriched in miR-143-3p, and to a lesser extent, the miR-143-5p passenger strand. Therefore, exosomes containing miR-143 and secreted by PAH-PASMCs might enhance the development of lesions associated with pulmonary hypertension and could be of clinical importance. Hence, cell:cell communication between compartments might be critical in the pathogenesis of PAH. We observed a reduction in microvessel density in the miR-143-/- hypoxic lungs compared to WT, suggesting that miR-143 transport in exosomes could enhance microvessel density and lung perfusion. Further experiments will be needed to address this effect *in vivo*.

MiRNAs are potential therapeutic targets for several diseases, including PAH. We have shown that miR-143, specifically localized to the SMC layers of pulmonary arteries in multiple models of disease is also significantly upregulated in human PAH patients.. The Brisket disease samples in particular share some common features of the human disease, including right heart failure and the development of complex vascular lung lesions. Since expression of miR-143 appears high in both acute (murine hypoxia-induced) and chronic (rat sugen/hypoxia and post-mortem human lung and brisket disease samples) samples, it suggests that miR-143 expression is elevated and sustained during the pathogenesis of PAH, particularly evident in distal small vessels (Figure 6 and Supplementary Figure S12). Also, miR-143 manipulation *in vitro* affected cell migration but not proliferation in both PASMCs and PAECs. Next, the chronic hypoxia PH mouse model demonstrated that genetic ablation of miR-143 prevents the development of PH. To further explore the therapeutic role of miR-143-3p, we performed pharmological manipulation of miR-143 in WT mice treated with antimiR. Genetic ablation and pharmacological inhibition of miR-143 exert a protective role in the development of PH. We previously reported that antimiR-143 did not signficantly reverse indices of PAH[17], however, there was a trend to lower RVSP. We clearly report here that both a prevention and reversal study show efficacy of the antimiR approach. The two results are not inconsistent with each other, due to the consistency in the direction of response and the current study having a greater power to declare genuine differences between groups as reaching statistical significance given its greater sample size. Ultimately, Caruso et

al[17] found insufficient evidence to conclude an involvement for miR-143 in development of PAH in experimental mice, but the larger sample sizes used in the current study have given us greater statistical power and allowed us to find statistically significant evidence as to the function and importance of miR-143.

In conclusion, we have, for the first time, performed detailed experimental characterisation of the promoter sequence controlling transcription of the miR-143/145 cluster, unravelling the most significant signalling pathways involved. Many of these signalling pathways have previously been implicated in the development of PAH, in which the expression of miR-143 is shown to be increased. Moreover, this is the first study to show that miRNAs are involved in the crosstalk between PASMCs and PAECs in PAH, suggesting that miR-143 may act as a crucial paracrine signalling mediator during remodeling of the pulmonary vasculature. Thus our study illustrates a novel role for miR-143-3p as therapeutic target in PAH.

ACKNOWLEDGMENTS

We would like to thank Dr. Eric N. Olson, PhD (University of Texas Southwestern Medical Center, TX) for kindly providing miR-143$^{-/-}$ mice, and Margaret Nilsen, Nicola Britton and Gregor Aitchison for technician support. We thank the Loughrey group (University of Glasgow) for mouse cardiomyocytes and fibroblasts.

SOURCES OF FUNDING

This work is supported by a Special Project grant from the British Heart Foundation (SP/12/9/29593) and China Scholarship Council (201206240013). Professor Andrew Baker is supported by the British Heart Foundation Chair of Translational Cardiovascular Sciences. Infrastructure support was provided by the Cambridge NIHR Biomedical Research Centre.

DISCLOSURES

No conflicts of interest, financial or otherwise, are declared by the authors.

REFERENCES

1. Thenappan T, Ryan JJ, Archer SL. Evolving epidemiology of pulmonary arterial hypertension. *Am J Respir Crit Care Med*. 2012;186:707-709
2. Tuder RM, Abman SH, Braun T, Capron F, Stevens T, Thistlethwaite PA, Haworth SG. Development and pathology of pulmonary hypertension. *J Am Coll Cardiol*. 2009;54:S3-9
3. Morrell NW, Adnot S, Archer SL, Dupuis J, Jones PL, MacLean MR, McMurtry IF, Stenmark KR, Thistlethwaite PA, Weissmann N, Yuan JX, Weir EK. Cellular and molecular basis of pulmonary arterial hypertension. *J Am Coll Cardiol*. 2009;54:S20-31
4. Austin ED, Lahm T, West J, Tofovic SP, Johansen AK, Maclean MR, Alzoubi A, Oka M. Gender, sex hormones and pulmonary hypertension. *Pulm Circ*. 2013;3:294-314

5. Upton PD, Davies RJ, Tajsic T, Morrell NW. Transforming growth factor-beta(1) represses bone morphogenetic protein-mediated smad signaling in pulmonary artery smooth muscle cells via smad3. *Am J Respir Cell Mol Biol*. 2013;49:1135-1145
6. Liu D, Morrell NW. Genetics and the molecular pathogenesis of pulmonary arterial hypertension. *Curr Hypertens Rep*. 2013;15:632-637
7. Bartel DP. Micrornas: Genomics, biogenesis, mechanism, and function. *Cell*. 2004;116:281-297
8. Saini HK, Griffiths-Jones S, Enright AJ. Genomic analysis of human microrna transcripts. *Proc Natl Acad Sci U S A*. 2007;104:17719-17724
9. Chien CH, Sun YM, Chang WC, Chiang-Hsieh PY, Lee TY, Tsai WC, Horng JT, Tsou AP, Huang HD. Identifying transcriptional start sites of human microrna based on high-throughput sequencing data. *Nucleic Acids Res*. 2011;39:9345-9356
10. Cordes KR, Sheehy NT, White MP, Berry EC, Morton SU, Muth AN, Lee TH, Miano JM, Ivey KN, Srivastava D. Mir-145 and mir-143 regulate smooth muscle cell fate and plasticity. *Nature*. 2009;460:705-710
11. Boettger T, Beetz N, Kostin S, Schneider J, Kruger M, Hein L, Braun T. Acquisition of the contractile phenotype by murine arterial smooth muscle cells depends on the mir143/145 gene cluster. *J Clin Invest*. 2009;119:2634-2647
12. Elia L, Quintavalle M, Zhang J, Contu R, Cossu L, Latronico MV, Peterson KL, Indolfi C, Catalucci D, Chen J, Courtneidge SA, Condorelli G. The knockout of mir-143 and -145 alters smooth muscle cell maintenance and vascular homeostasis in mice: Correlates with human disease. *Cell Death Differ*. 2009;16:1590-1598
13. Lovren F, Pan Y, Quan A, Singh KK, Shukla PC, Gupta N, Steer BM, Ingram AJ, Gupta M, Al-Omran M, Teoh H, Marsden PA, Verma S. Microrna-145 targeted therapy reduces atherosclerosis. *Circulation*. 2012;126:S81-90
14. Hutcheson R, Terry R, Chaplin J, Smith E, Musiyenko A, Russell JC, Lincoln T, Rocic P. Microrna-145 restores contractile vascular smooth muscle phenotype and coronary collateral growth in the metabolic syndrome. *Arterioscler Thromb Vasc Biol*. 2013;33:727-736
15. Fichtlscherer S, De Rosa S, Fox H, Schwietz T, Fischer A, Liebetrau C, Weber M, Hamm CW, Roxe T, Muller-Ardogan M, Bonauer A, Zeiher AM, Dimmeler S. Circulating microrna in patients with coronary artery disease. *Circ Res*. 2010;107:677-684
16. Cheng Y, Liu X, Yang J, Lin Y, Xu DZ, Lu Q, Deitch EA, Huo Y, Delphin ES, Zhang C. Microrna-145, a novel smooth muscle cell phenotypic marker and modulator, controls vascular neointimal lesion formation. *Circ Res*. 2009;105:158-166
17. Caruso P, Dempsie Y, Stevens HC, McDonald RA, Long L, Lu R, White K, Mair KM, McClure JD, Southwood M, Upton P, Xin M, van Rooij E, Olson EN, Morrell NW, MacLean MR, Baker AH. A role for mir-145 in pulmonary arterial hypertension: Evidence from mouse models and patient samples. *Circ Res*. 2012;111:290-300
18. Valadi H, Ekstrom K, Bossios A, Sjostrand M, Lee JJ, Lotvall JO. Exosome-mediated transfer of mrnas and microrna is a novel mechanism of genetic exchange between cells. *Nat Cell Biol*. 2007;9:654-659
19. Thery C, Ostrowski M, Segura E. Membrane vesicles as conveyors of immune responses. *Nat Rev Immunol*. 2009;9:581-593
20. Hergenreider E, Heydt S, Treguer K, Boettger T, Horrevoets AJ, Zeiher AM, Scheffer MP, Frangakis AS, Yin X, Mayr M, Braun T, Urbich C, Boon RA, Dimmeler S. Atheroprotective communication between endothelial cells and smooth muscle cells through mirnas. *Nat Cell Biol*. 2012;14:249-256
21. Loyer X, Vion AC, Tedgui A, Boulanger CM. Microvesicles as cell-cell messengers in cardiovascular diseases. *Circ Res*. 2014;114:345-353
22. Garrido-Martin EM, Blanco FJ, Roque M, Novensa L, Tarocchi M, Lang UE, Suzuki T, Friedman SL, Botella LM, Bernabeu C. Vascular injury triggers kruppel-like factor 6 mobilization and

cooperation with specificity protein 1 to promote endothelial activation through upregulation of the activin receptor-like kinase 1 gene. *Circ Res*. 2013;112:113-127
23. Yang J, Li X, Li Y, Southwood M, Ye L, Long L, Al-Lamki RS, Morrell NW. Id proteins are critical downstream effectors of bmp signaling in human pulmonary arterial smooth muscle cells. *Am J Physiol Lung Cell Mol Physiol*. 2013;305:L312-321
24. White K, Johansen AK, Nilsen M, Ciuclan L, Wallace E, Paton L, Campbell A, Morecroft I, Loughlin L, McClure JD, Thomas M, Mair KM, MacLean MR. Activity of the estrogen-metabolizing enzyme cytochrome p450 1b1 influences the development of pulmonary arterial hypertension. *Circulation*. 2012;126:1087-1098
25. Lefebvre P, Benomar Y, Staels B. Retinoid x receptors: Common heterodimerization partners with distinct functions. *Trends Endocrinol Metab*. 2010;21:676-683
26. Genomes Project C, Abecasis GR, Auton A, Brooks LD, DePristo MA, Durbin RM, Handsaker RE, Kang HM, Marth GT, McVean GA. An integrated map of genetic variation from 1,092 human genomes. *Nature*. 2012;491:56-65
27. Shimbo K, Miyaki S, Ishitobi H, Kato Y, Kubo T, Shimose S, Ochi M. Exosome-formed synthetic microrna-143 is transferred to osteosarcoma cells and inhibits their migration. *Biochem Biophys Res Commun*. 2014;445:381-387
28. Jordan SD, Kruger M, Willmes DM, Redemann N, Wunderlich FT, Bronneke HS, Merkwirth C, Kashkar H, Olkkonen VM, Bottger T, Braun T, Seibler J, Bruning JC. Obesity-induced overexpression of mirna-143 inhibits insulin-stimulated akt activation and impairs glucose metabolism. *Nat Cell Biol*. 2011;13:434-446
29. Xin M, Small EM, Sutherland LB, Qi X, McAnally J, Plato CF, Richardson JA, Bassel-Duby R, Olson EN. Micrornas mir-143 and mir-145 modulate cytoskeletal dynamics and responsiveness of smooth muscle cells to injury. *Genes Dev*. 2009;23:2166-2178
30. Mair KM, Johansen AK, Wright AF, Wallace E, MacLean MR. Pulmonary arterial hypertension: Basis of sex differences in incidence and treatment response. *Br J Pharmacol*. 2014;171:567-579
31. Valbuena-Diez AC, Blanco FJ, Oujo B, Langa C, Gonzalez-Nunez M, Llano E, Pendas AM, Diaz M, Castrillo A, Lopez-Novoa JM, Bernabeu C. Oxysterol-induced soluble endoglin release and its involvement in hypertension. *Circulation*. 2012;126:2612-2624
32. Choudhry H, Schodel J, Oikonomopoulos S, Camps C, Grampp S, Harris AL, Ratcliffe PJ, Ragoussis J, Mole DR. Extensive regulation of the non-coding transcriptome by hypoxia: Role of hif in releasing paused rnapol2. *EMBO Rep*. 2014;15:70-76
33. Zuo L, Rose BA, Roberts WJ, He F, Banes-Berceli AK. Molecular characterization of reactive oxygen species in systemic and pulmonary hypertension. *Am J Hypertens*. 2014;27:643-650
34. Mayorga ME, Penn MS. Mir-145 is differentially regulated by tgf-beta1 and ischaemia and targets disabled-2 expression and wnt/beta-catenin activity. *J Cell Mol Med*. 2012;16:1106-1113
35. Humbert M, Morrell NW, Archer SL, Stenmark KR, MacLean MR, Lang IM, Christman BW, Weir EK, Eickelberg O, Voelkel NF, Rabinovitch M. Cellular and molecular pathobiology of pulmonary arterial hypertension. *J Am Coll Cardiol*. 2004;43:13S-24S
36. Archer SL, Weir EK, Wilkins MR. Basic science of pulmonary arterial hypertension for clinicians: New concepts and experimental therapies. *Circulation*. 2010;121:2045-2066
37. Grant JS, White K, MacLean MR, Baker AH. Micrornas in pulmonary arterial remodeling. *Cell Mol Life Sci*. 2013;70:4479-4494
38. Treguer K, Heinrich EM, Ohtani K, Bonauer A, Dimmeler S. Role of the microrna-17-92 cluster in the endothelial differentiation of stem cells. *J Vasc Res*. 2012;49:447-460
39. Ma Q, Jiang Q, Pu Q, Zhang X, Yang W, Wang Y, Ye S, Wu S, Zhong G, Ren J, Zhang Y, Liu L, Zhu W. Microrna-143 inhibits migration and invasion of human non-small-cell lung cancer and its relative mechanism. *Int J Biol Sci*. 2013;9:680-692

40. Xu B, Niu X, Zhang X, Tao J, Wu D, Wang Z, Li P, Zhang W, Wu H, Feng N, Wang Z, Hua L, Wang X. Mir-143 decreases prostate cancer cells proliferation and migration and enhances their sensitivity to docetaxel through suppression of kras. *Mol Cell Biochem*. 2011;350:207-213
41. Wang L, Xiong H, Wu F, Zhang Y, Wang J, Zhao L, Guo X, Chang LJ, You MJ, Koochekpour S, Saleem M, Huang H, Lu J, Deng Y. Hexokinase 2-mediated warburg effect is required for pten- and p53-deficiency-driven prostate cancer growth. *Cell Rep*. 2014;8:1461-1474
42. Bang C, Batkai S, Dangwal S, Gupta SK, Foinquinos A, Holzmann A, Just A, Remke J, Zimmer K, Zeug A, Ponimaskin E, Schmiedl A, Yin X, Mayr M, Halder R, Fischer A, Engelhardt S, Wei Y, Schober A, Fiedler J, Thum T. Cardiac fibroblast-derived microrna passenger strand-enriched exosomes mediate cardiomyocyte hypertrophy. *J Clin Invest*. 2014;124:2136-2146
43. Sahoo S, Losordo DW. Exosomes and cardiac repair after myocardial infarction. *Circ Res*. 2014;114:333-344

FIGURE LEGENDS

Figure 1. Analysis of the miR143/145 promoter. (**A**) Scheme of a 1.5 kb region of the proximal promoter. Homology percentage among species is indicated (with arrows). Transcription factor binding sites are shown as arrow heads above/below the line if located in the plus/minus strand respectively. (**B**-**E**) Estradiol (E2) at 10 nM for 24 hours induced the expression of pri-miR-143/145 (**B**), mature miR-143/145 but not their passenger strands miR143*(miR-143-5p)/145*(miR-145-3p) in PASMC (**C**), and transcriptional activity of the full length promoter p1.5-luc and proximal promoter p0.5-luc in HeLa cells (**D**), dependent on sites located at (-801) and (-14) (**E**). (**F**-**I**) LXR/RXR pathway was induced by 9cRA and 22R (5 μM each) for 24 hours in PASMC. The expression levels of pri-miR-143/145 (**F**) and mature miR-143/145 and miR-143*/145* (**G**) were detected by qPCR. Transcriptional activity of the promoter was assayed in HeLa cells (**H**-**I**). (**J**-**M**) Exposure to hypoxia (1% O_2 for 24 hours) increased the expression of pri-miR-143/145 (**J**), and miR-143/145 and miR-143* in PASMC (**K**). Transcriptional activity was dependent on the hypoxia response element (HRE) located at (-113) (**M**). *$p < 0.05$, **$p < 0.01$ and ***$p<0.005$.

Figure 2. Analysis of the TGF-β pathway in PASMC. (**A**-**B**) Pri-miR-143/145 and all four mature forms miR143/145 and miR143*/145* were upregulated by 10 ng/ml TGF-β1 for 24 hours, but no effect was detected after BMP4 treatment. (**C**) Transcriptional activation of the miR-143/145 promoter was induced by TGF-β1 only in the full length p1.5-luc reporter. (**D**) Site-directed mutagenesis demonstrated the relevance of the Smad binding site at (-592). (**E**-**F**) Decoy assay for the Smad3 binding site using phosphorothioate oligodeoxynucleotides (PTO-ODN). Only the wild type decoy and not those bearing Smad3 SNPs (rs12517403 and rs116423755) inhibits the TGF-β1-induced pri-miR-143/145 (**E**) and mature miR-143/145 (**F**) expression. *$p < 0.05$, **$p < 0.01$ and ***$p<0.005$.

Figure 3. Manipulation of miR-143/145 cluster affects PASMC migration. Expression levels of pri-miR-143 and pri-miR-145 (**A**), mature miR-143-3p and miR-145-5p (**B**) and their respective passenger strands miR-143* (miR-143-5p) and miR-145* (miR-145-3p) (**C**) during scratch closure of PASMC by qPCR. (**D**) Representative micrographs and quantification of a wound healing assay after miR-143 overexpression by pre-miR-143 transfection, in comparison with vehicle and negative control (NC). MiR-143 Expression relative to control by qPCR is shown (**E**). (**F,G**) Representative micrographs of a wound healing assay after miR-143 knock-down by specific antimiRNA, compared with vehicle or negative control (NC). MiR-143 xpression relative to control by qPCR is shown (**G**). (**H**-**J**) Wound healing assay with PASMC nucleofected with a GFP reporter in which expression is driven by the miR-143/145 promoter mainly in cells migrating from the border of the scratch. All experiments were repeated at least 3 independent times. *$p < 0.05$, **$p < 0.01$ and ***$p<0.005$.

Figure 4. Extracellular miR-143 from PASMCs is transferred to PAEs and induces their migration (**A**) Diagram of the transwell used for the *in vitro* co-culture system. (**B**) PASMCs were transfected with Cy3-pre-miRNA in the upper chamber. Cy3-labeled, miRNA-enriched exosomes are then released and transferred to PAEC in the lower chamber after 24 hours (n=3). (**C**) Co-culture system applied with PASMCs (insert) and PAECs (bottom) for 48 hours to assess the endogenously transfer of miR-143 from PASMCs to PAECs, Q-PCR showed the miR-143 expression level in PAECs after co-culture compared with control (n=6). (D) PASMCs were transfected with pre-miR-143 or negative control (NC), co-cultured with PAECs for 24 or 48 hours, and expression of miR-143 was measured in PASMCs and PAECs by qPCR (n=3). (**E**) Representative micrographs and relative migration distance of PAEC migration during scratch closure in co-culture with pre-miR-143-transfected PASMC. (**F**) Q-PCR showed the expression level of miR-143 in PAECs (n=3). (**G**) Representative micrographs and relative migration distance of PAEC migration during scratch closure with conditioned medium from transfected PASMCs. (**H**) Q-PCR show the expression level of miR-143 in PAECs. (n = 3) *$p < 0.05$, **$p < 0.01$ and ***$p < 0.005$.

Figure 5. Released functional extracellular miR-143 in exosomes (**A**) Taqman qPCR Ct value showed miR-143 expression in PASMC and PASMC-derived exosomes. (**B**) The exosome pellet was re-suspended in PBS and visualized on the NanoSight instrument. The analysis shows the size of isolated exosomes is between 30-130nm. (C) Western Blot of PASMC-derived exosomes for CD63, CD9 and GAPDH. (**D**-**E**) Q-PCR analysis of miR-143 expression in PASMCs and PASMC-derived exosomes after the cells were transfected with negative control or pre-miR143 (10nM, 50nM and 100nM). RNU48 and cel-miR-39 were used as internal loading controls for cells and exosomes respectively (n=3). (**F**) Representative micrographs and relative migration distance of PAECs during scratch closure, after treatment with isolated exosomes derived from PASMCs transfected with pre-miR-143, vehicle or negative control (NC). (**G**) Q-PCR showing the expression level of miR-143 in exosomes (n=3). (**H**) Representative micrographs and relative migration distance of PAECs during scratch closure after direct transfection with pre-miR143. (**I**) Q-PCR showing the expression level of miR-143 in PAECs. (n=3) (**J**) Matrigel angiogenesis assay in PAECs transfected with pre-miR-143 or loaded with miR-143 enriched exosomes. Images ×10 magnification, scale bar represents 250μm (n=3). (**K**) Quantification of total tube lengths in PAECS treated with exosomes from pre-miR-143 transfected PASMCs (**L**) Quantification of total tube lengths in PAECS transfected with pre-miR-143. *p<0.05 and **p< 0.01, ***$p < 0.005$.

Figure 6. MiR-143 expression is upregulated in experimental models of PH. Quantitative PCR analyses of miR-143 stem-loop in total lung (**A**) and right ventricle (**B**) of normoxic and hypoxic mice (n=6) were analyzed for miR-143 expression by qPCR. Results were normalized to U6 values. (**C**) MiR-143 stem-loop expression in PASMC from female PAH patients and healthy controls by qPCR (n=7). (**D**) *In situ* hybridization of hypoxic neonatal calf and Brisket Disease calves show increased expression of miR-143 compared with healthy controls. (**E**) *In situ* hybridization of human lung of pulmonary vessels revealed increased miR-143 localized in the smooth muscle layer of constrictive and complex arterial lesions of PAH patients. Scale bar = 100 μm. *$p < 0.05$, **$p < 0.01$ and ***$p < 0.001$.

Figure 7. Direct knockout of miR-143 stem loop and pharmacological inhibition of miR-143-3p in mice alleviates the development of PH *in vivo*. (A) Analysis of SAP, (**B**) Assessment of systolic right ventricular pressure (sRVP, n= 9-12) (**C**), and right ventricular hypertrophy (RVH, n=12) in WT and miR-143 KO mice after 14 days hypoxic exposure. (**D**) Distal pulmonary artery vessel wall thickness and remodelling were analyzed by α-smooth muscle actin (α-SMC) and CD31 staining in

miR-143 KO mice compared with their WT littermate controls in both normoxia and hypoxia condition (n=4, scale bar=20 μ m). (**E**) Prevention model with pharmacological inhibition of miR-143-3p in mice exposed to chronic hypoxia and in normoxic controls. (**F**) Systolic right ventricular pressure (RVP, n=10-17) and (**G**) right ventricular hypertrophy (RVH, n=10-17) and (**H**) SAP were measured in normoxia and hypoxia in vehicle, scramble anti-miRNA and anti-miR-143 mice groups (n=10-17). (**I**) Hypoxia rescue model with pharmacological inhibition of miR-143-3p in mice exposed to chronic hypoxia. (**J**) Systolic right ventricular pressure (RVP, n=7-9) and (**K**) right ventricular hypertrophy (RVH, n=10), (L) SAP (n=5/group) were measured. *$p < 0.01$, **$p < 0.01$, ***$p < 0.001$.

Figure 8. Model of the regulation and actions of the miR-143/145 cluster in PAH. Several signalling pathways related to the pathogenesis of PAH regulate miR-143/145 expression by activating the promoter region of the miR-143/145 cluster in PASMCs. MiR-143-3p can affect cellular migration and apoptosis and acts as a paracrine signalling mediator during vascular remodelling. During the development of PAH, PASMCs secrete exosomes enriched with miR-143-3p, which are transported to PAEC, inducing migration and angiogenesis.

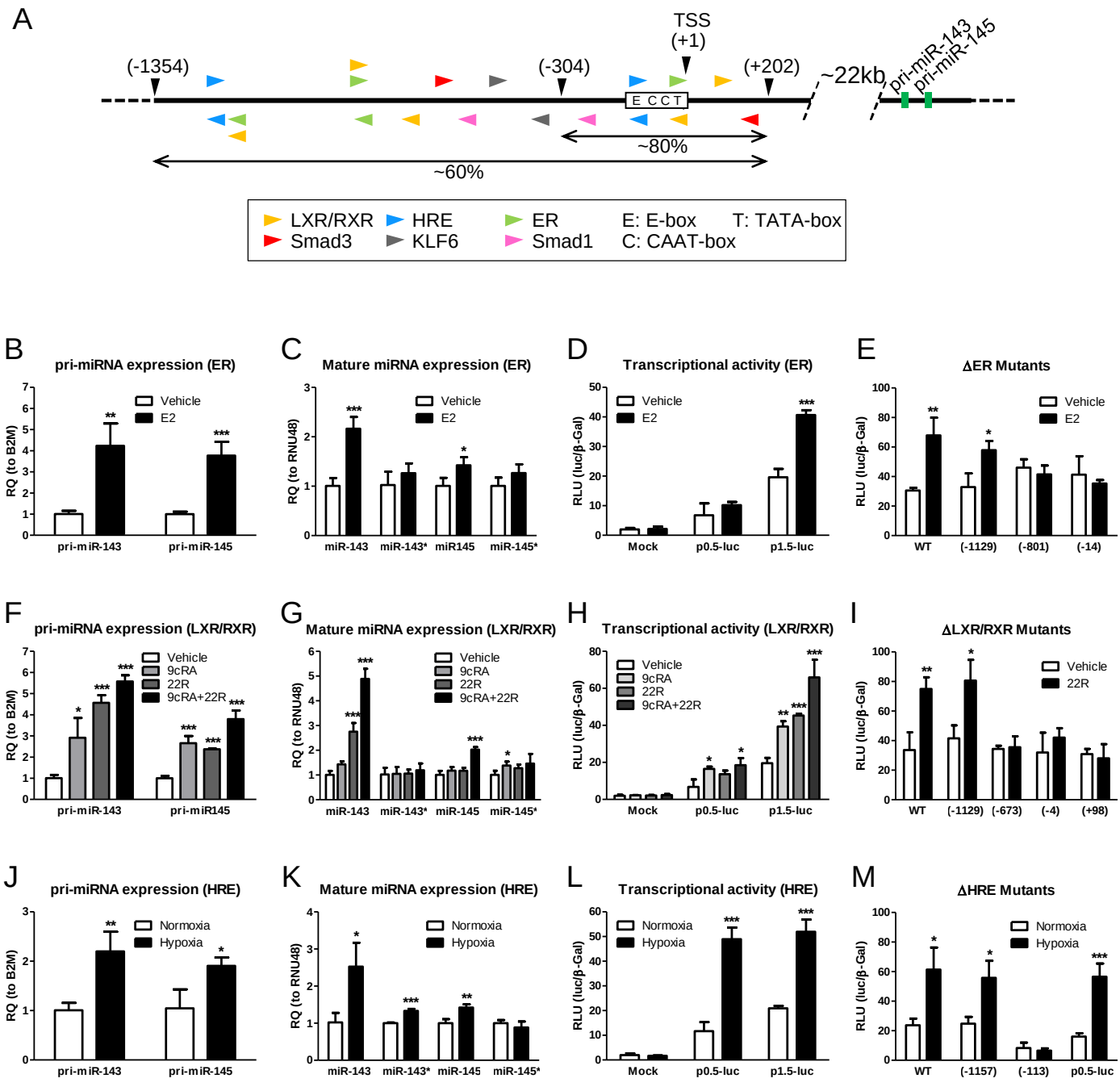
A
TSS
(+1)
(-1354)
(-304)
(+202)
~22kb
pri-miR-143
pri-miR-145
E C C T
~80%
~60%
LXR/RXR
HRE
ER
E: E-box
T: TATA-box
Smad3
KLF6
Smad1
C: CAAT-box
B
pri-miRNA expression (ER)
RQ (to B2M)
Vehicle
E2
pri-miR-143
pri-miR-145
C
Mature miRNA expression (ER)
RQ (to RNU48)
miR-143
miR-143*
miR145
miR-145*
D
Transcriptional activity (ER)
RLU (luc/β-Gal)
Mock
p0.5-luc
p1.5-luc
E
ΔER Mutants
WT
(-1129)
(-801)
(-14)
F
pri-miRNA expression (LXR/RXR)
9cRA
22R
9cRA+22R
pri-miR145
G
Mature miRNA expression (LXR/RXR)
H
Transcriptional activity (LXR/RXR)
I
ΔLXR/RXR Mutants
(-673)
(-4)
(+98)
J
pri-miRNA expression (HRE)
Normoxia
Hypoxia
K
Mature miRNA expression (HRE)
L
Transcriptional activity (HRE)
M
ΔHRE Mutants
(-1157)
(-113)

Figure 1

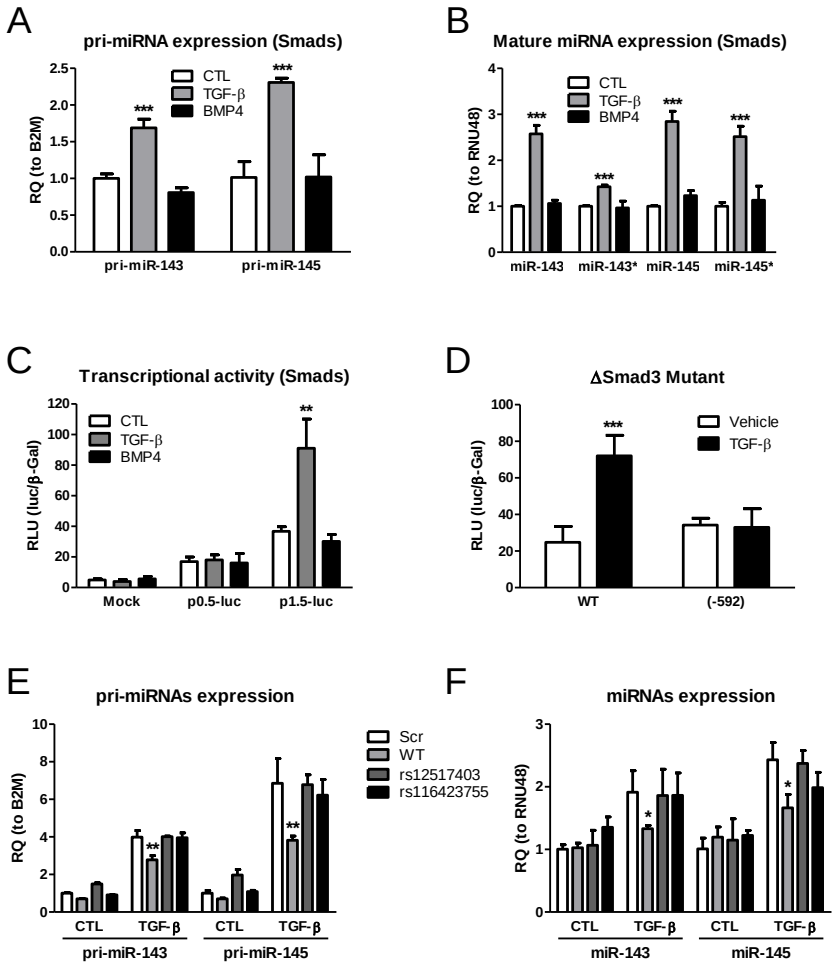
A
pri-miRNA expression (Smads)
RQ (to B2M)
CTL
TGF-β
BMP4
pri-miR-143
pri-miR-145
B
Mature miRNA expression (Smads)
RQ (to RNU48)
miR-143
miR-143*
miR-145
miR-145*
C
Transcriptional activity (Smads)
RLU (luc/β-Gal)
Mock
p0.5-luc
p1.5-luc
D
ΔSmad3 Mutant
Vehicle
TGF-β
WT
(-592)
E
pri-miRNAs expression
Scr
WT
rs12517403
rs116423755
F
miRNAs expression

Figure 2

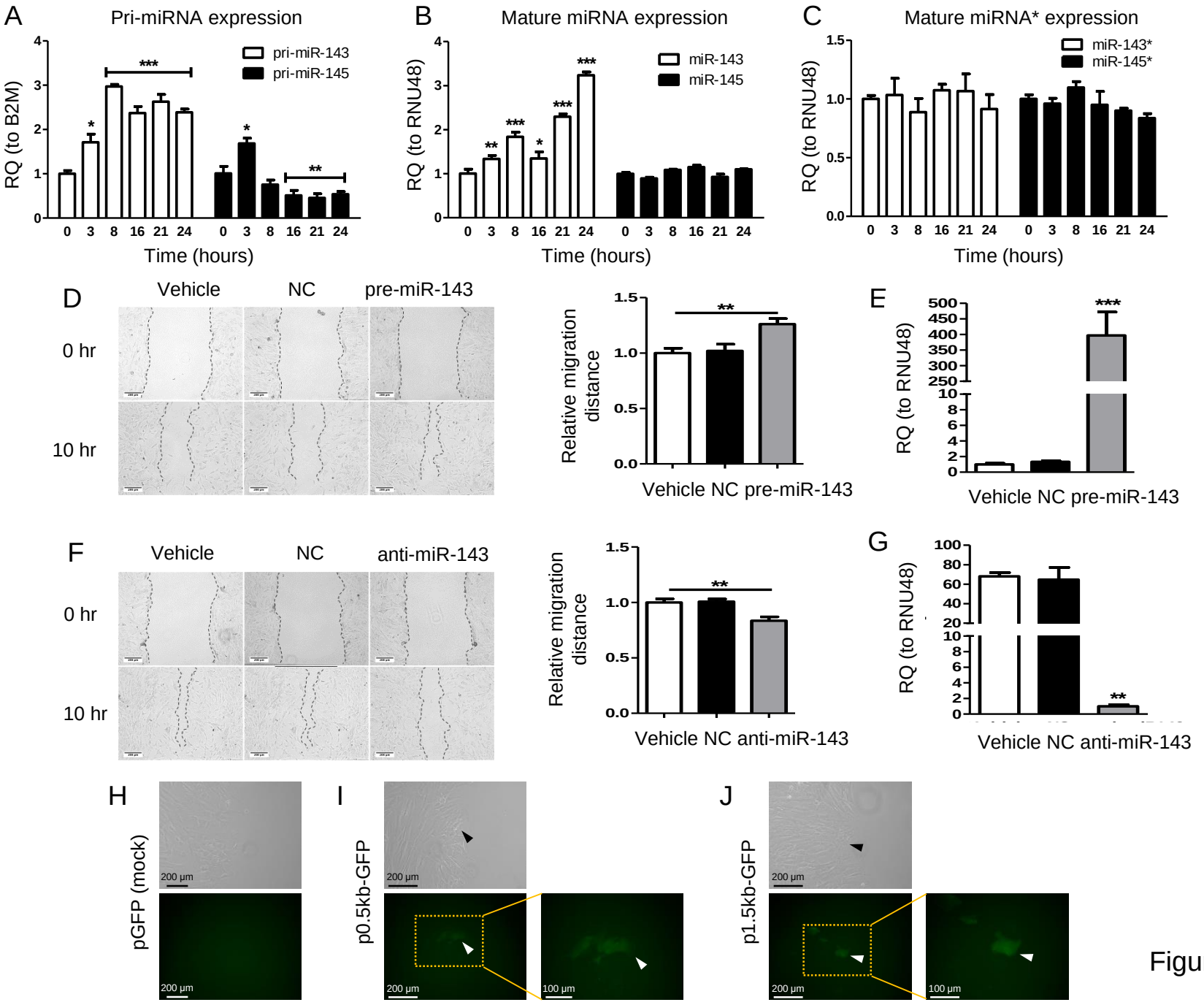
A
Pri-miRNA expression
RQ (to B2M)
pri-miR-143
pri-miR-145
Time (hours)
B
Mature miRNA expression
RQ (to RNU48)
miR-143
miR-145
Time (hours)
C
Mature miRNA* expression
RQ (to RNU48)
miR-143*
miR-145*
Time (hours)
D
Vehicle
NC
pre-miR-143
0 hr
10 hr
Relative migration distance
Vehicle NC pre-miR-143
E
RQ (to RNU48)
Vehicle NC pre-miR-143
F
Vehicle
NC
anti-miR-143
0 hr
10 hr
Relative migration distance
Vehicle NC anti-miR-143
G
RQ (to RNU48)
Vehicle NC anti-miR-143
H
pGFP (mock)
I
p0.5kb-GFP
J
p1.5kb-GFP
200 μm
100 μm

Figure 3

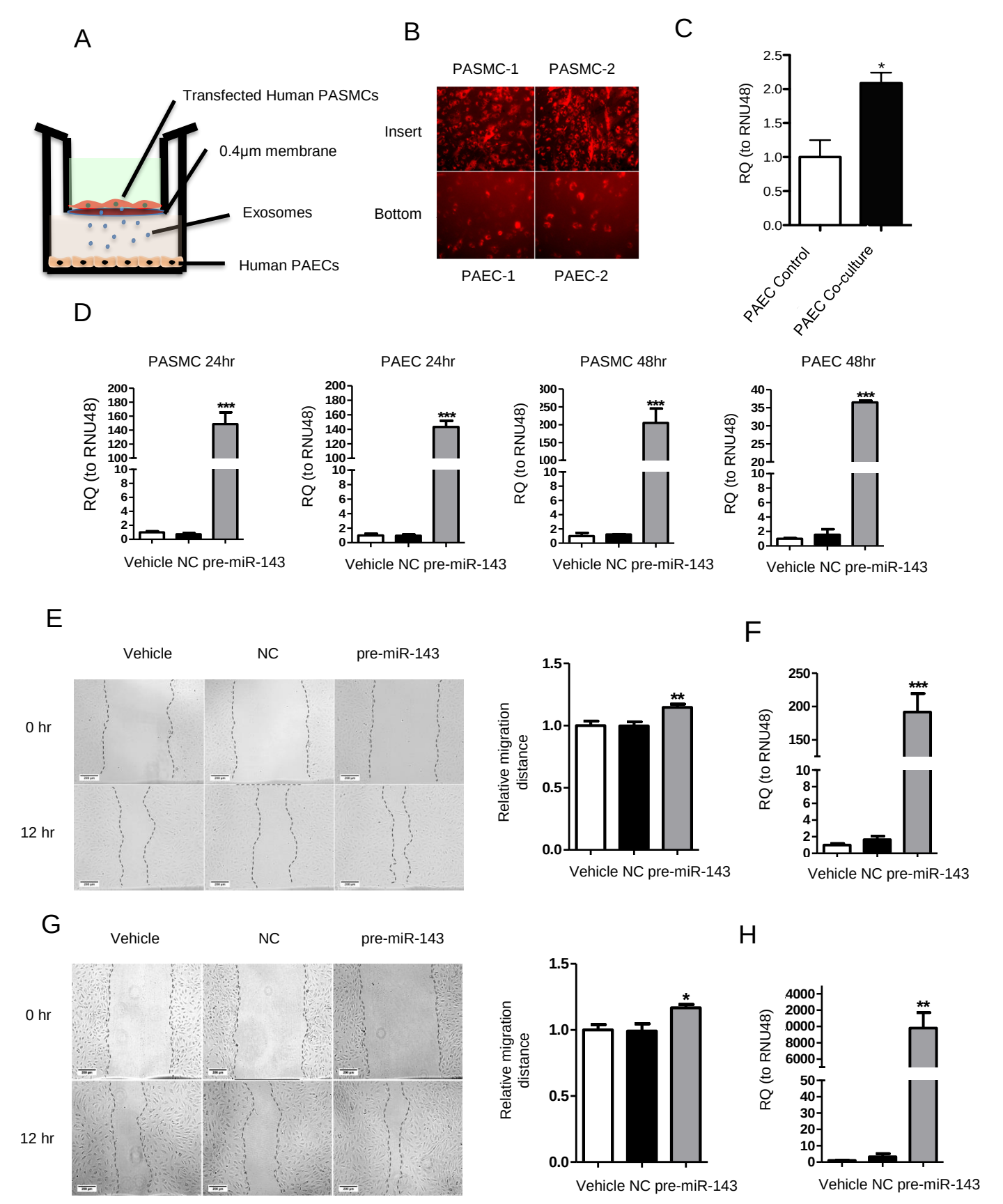
A
Transfected Human PASMCs
0.4μm membrane
Exosomes
Human PAECs
B
PASMC-1
PASMC-2
Insert
Bottom
PAEC-1
PAEC-2
C
RQ (to RNU48)
PAEC Control
PAEC Co-culture
D
PASMC 24hr
PAEC 24hr
PASMC 48hr
PAEC 48hr
RQ (to RNU48)
Vehicle NC pre-miR-143
E
Vehicle
NC
pre-miR-143
0 hr
12 hr
Relative migration distance
Vehicle NC pre-miR-143
F
RQ (to RNU48)
Vehicle NC pre-miR-143
G
Vehicle
NC
pre-miR-143
0 hr
12 hr
Relative migration distance
Vehicle NC pre-miR-143
H
RQ (to RNU48)
Vehicle NC pre-miR-143

Figure 4

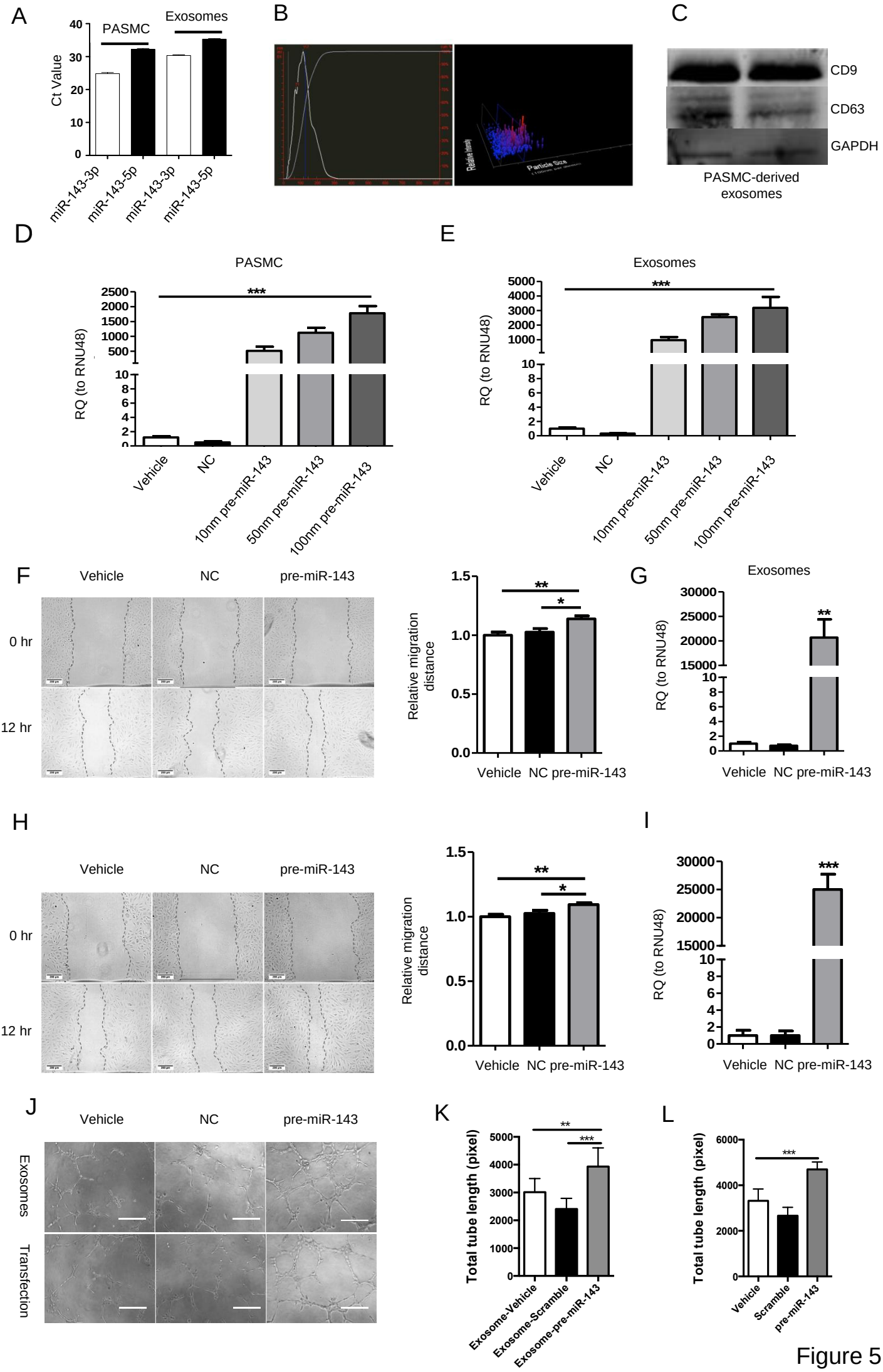
A
PASMC
Exosomes
Ct Value
miR-143-3p
miR-143-5p
miR-143-3p
miR-143-5p
B
C
CD9
CD63
GAPDH
PASMC-derived exosomes
D
PASMC
RQ (to RNU48)
Vehicle
NC
10nm pre-miR-143
50nm pre-miR-143
100nm pre-miR-143
E
Exosomes
RQ (to RNU48)
F
Vehicle
NC
pre-miR-143
0 hr
12 hr
Relative migration distance
G
Exosomes
RQ (to RNU48)
H
I
J
Exosomes
Transfection
K
Total tube length (pixel)
Exosome-Vehicle
Exosome-Scramble
Exosome-pre-miR-143
L
Total tube length (pixel)
Vehicle
Scramble
pre-miR-143

Figure 5

A

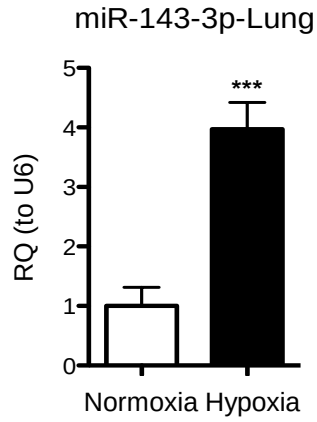

B

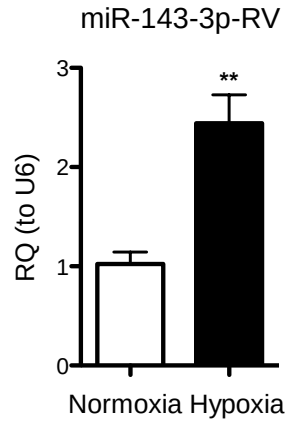

C

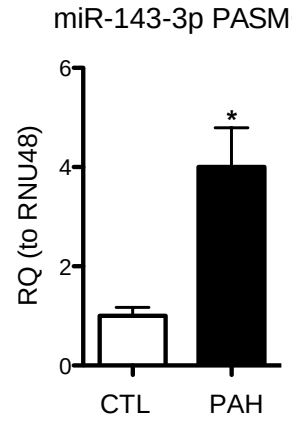

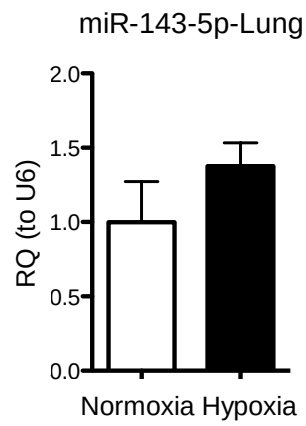

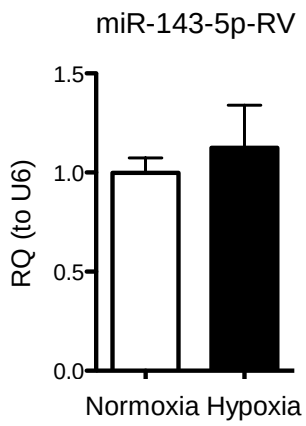

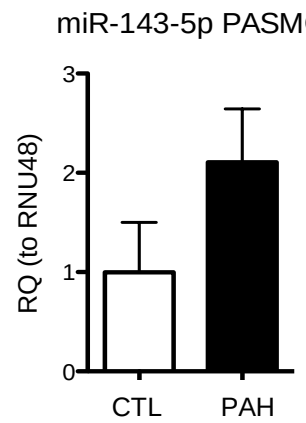

D

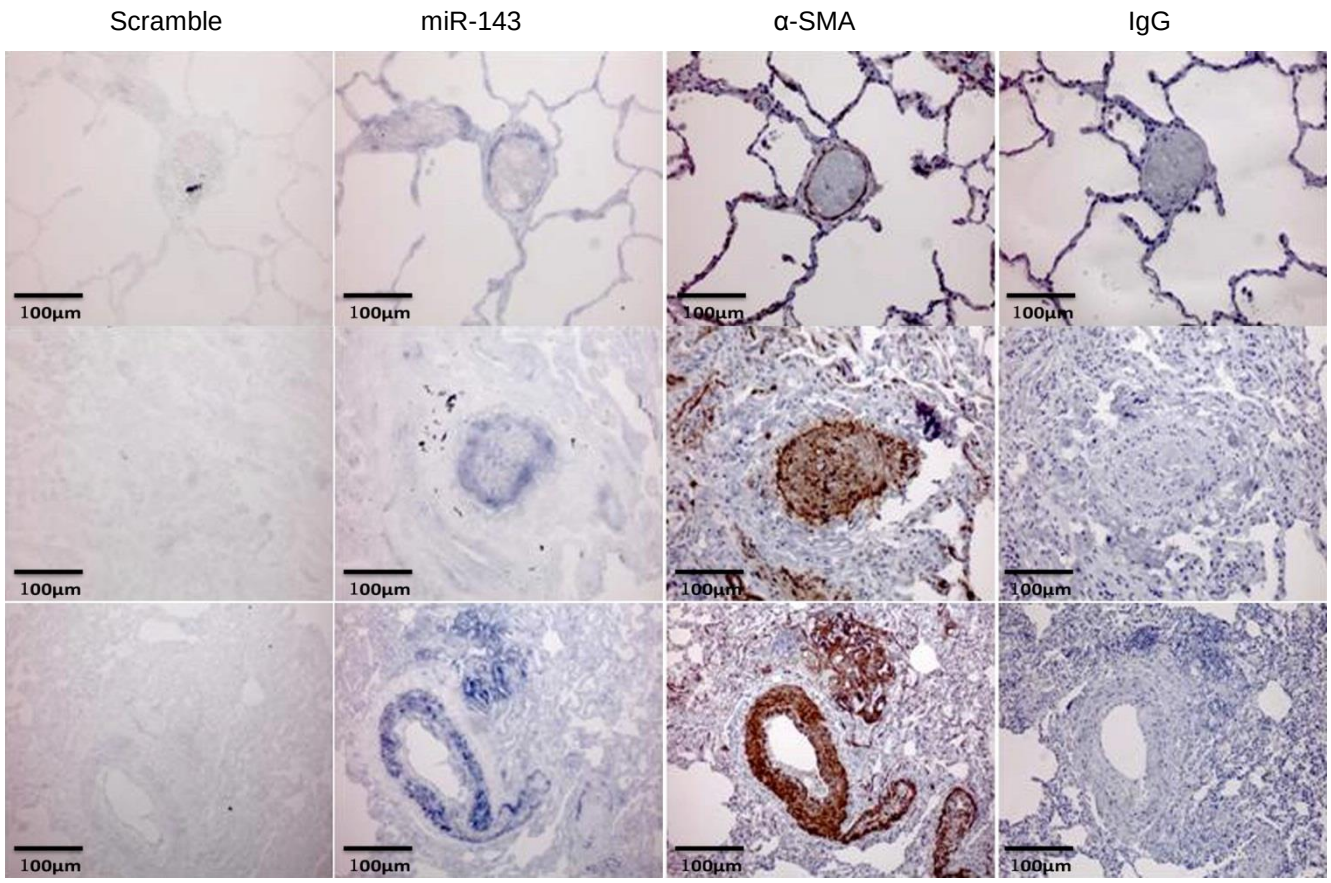

E

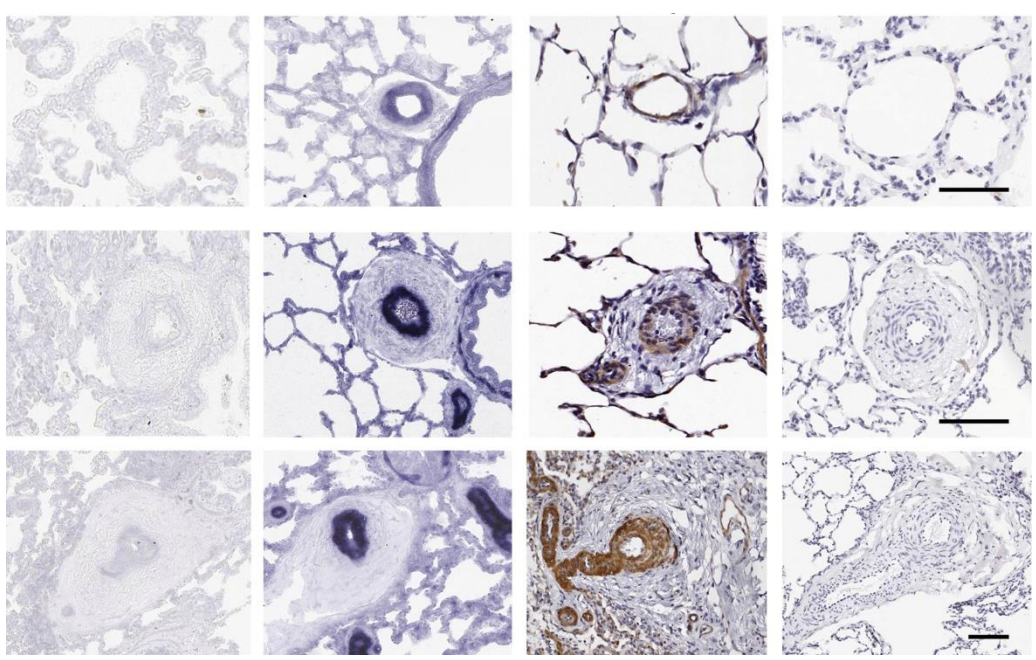

Figure 6

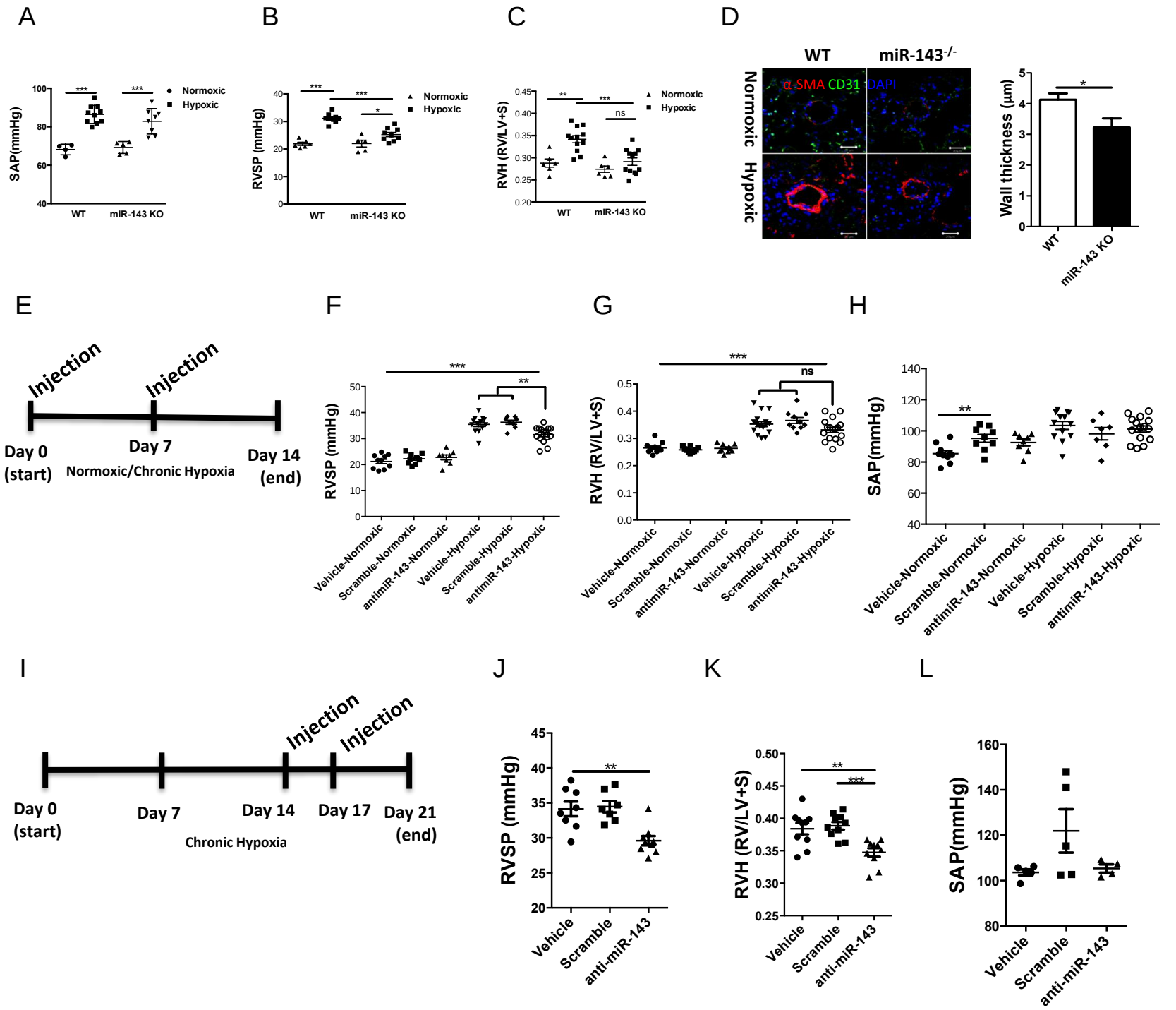
A
B
C
D
SAP(mmHg)
RVSP (mmHg)
RVH (RV/LV+S)
Normoxic
Hypoxic
WT
miR-143 KO
WT
miR-143-/-
α-SMA CD31 DAPI
Wall thickness (μm)
E
Injection
Injection
Day 0
(start)
Day 7
Normoxic/Chronic Hypoxia
Day 14
(end)
F
G
H
Vehicle-Normoxic
Scramble-Normoxic
antimiR-143-Normoxic
Vehicle-Hypoxic
Scramble-Hypoxic
antimiR-143-Hypoxic
I
Injection
Injection
Day 0
(start)
Day 7
Day 14
Day 17
Day 21
(end)
Chronic Hypoxia
J
K
L
Vehicle
Scramble
anti-miR-143

Figure 7

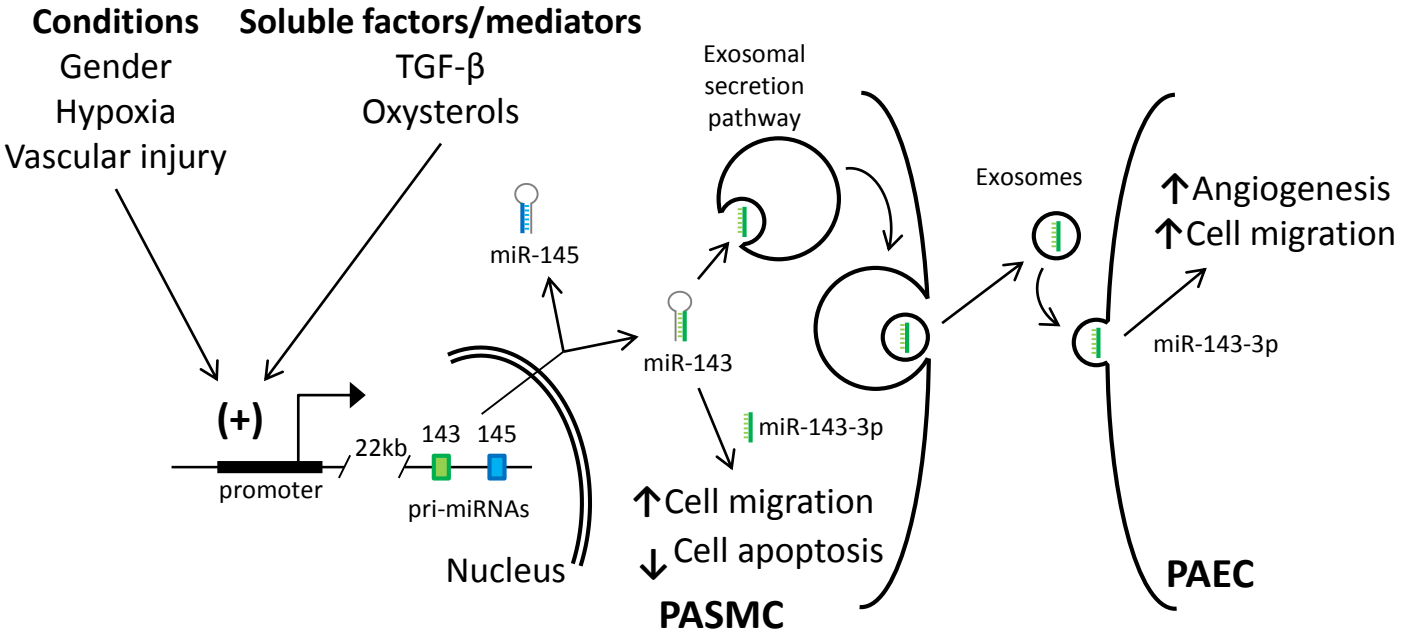
Conditions
Gender
Hypoxia
Vascular injury
Soluble factors/mediators
TGF-β
Oxysterols
(+)
promoter
22kb
143
145
pri-miRNAs
Nucleus
miR-145
miR-143
Exosomal
secretion
pathway
miR-143-3p
↑Cell migration
↓Cell apoptosis
PASMC
Exosomes
↑Angiogenesis
↑Cell migration
miR-143-3p
PAEC

Figure 8

SUPPLEMENTAL MATERIAL

MiR-143 activation regulates smooth muscle and endothelial cell crosstalk in pulmonary arterial hypertension

Short Title: Regulation and role of miR-143 in PAH

Lin Deng, Francisco J. Blanco, Hannah Stevens, Ruifang Lu, Axelle Caudrillier, Martin McBride, John D McClure, Jenny Grant, Matthew Thomas, Maria Frid, Kurt Stenmark, Kevin White, Anita G. Seto, Nicholas W. Morrell, Angela C Bradshaw, Margaret R. MacLean, Andrew H. Baker

Detailed Methods

Cloning the MIR143HG proximal promoter and reporter vectors

The location of the theoretical transcription start site (TSS) and proximal promoter region of the miR-143/145 hosting gene (*MIR143HG*) in chromosome 5 was predicted by the miRStart tool (http://mirstart.mbc.nctu.edu.tw/)[1]. Homologous sequences from different species were obtained from Ensembl database (http://www.ensembl.org) and analyzed with Clustal Omega at European Bioinformatics Institute website (http://www.ebi.ac.uk/Tools/msa/clustalo/). The *in silico* analysis of regulatory *cis*-elements was further carried out with MatInspector (Genomatix software suite, http://www.genomatix.de). Then, a primer pair was designed to amplify by PCR a spanning sequence of 1556 bp from a human genomic DNA sample: Fw(-1354): 5'-acgcgttgggggtctgaggaactgt; and Rv(+202): 5'-agatctctttcctggggtctggtcc, bearing a *Mlu*I and *Bgl*II targets in the 5'-end, respectively (underlined). In parallel, a minimal construction of 506 bp was also generated using an alternative *Mlu*I-targeted forward primer Fw(-304): 5'-acgcgttgcctccctctctcccct. Then, both PCR products were TA-cloned into pCR2.1-TOPO (Invitrogen, Paisley, UK), double digested with *Mlu*I/*Bgl*II and finally cloned into pGL3 basic vector (Promega, Madison, WI, USA) to generate p1.5-Luc and p0.5-Luc vectors, respectively.

In addition, these pGL3 reporter vectors were cleaved by *Kpn*I and *Bgl*II. Fragments were purified and oriented cloned into the promoterless pLenti-GFP reporter plasmid using its *Kpn*I and *Bam*HI sites, as *Bgl*II and *Bam*HI produce compatible ends. Final constructions were confirmed by sequencing. Thus, these plasmids and the corresponding empty vector were transferred into PASMC

by nucleofection (Amaxa, Köln, Germany), where the reporter expression of GFP is driven by that promoter sequence cloned upstream. No lentivirus is generated in this assay as these reporter vectors are used without the corresponding partner plasmids.

Cell culture and reagents

Primary culture of female proximal pulmonary artery smooth muscle cells (PASMCs) and pulmonary arterial endothelial cells (PAECs) were purchased from Lonza and grown in Clonetics SmGM-s BulletKit medium and EBM-2 Endothelial Growth Basal Medium, respectively (Lonza, Walkersville, MD, USA). Distal female PASMC from PAH patients were obtained from the Prof. Nicholas W. Morrell's lab (Addenbrooke's Hospital, University of Cambridge) and maintained in SmGM-s medium. Cells were used in early passages and maintained in exponential growth. For hypoxic exposure cells were placed into a hypoxic chamber (1% O_2, 5% CO_2, balance N_2) for 24 hours. Human epithelial HeLa cells were grown in Eagle's Minimum Essential Medium (Gibco, Paisley, UK) plus 10% FBS supplemented with 1 mM sodium pyruvate, 2 mM L-glutamine, and 100 U/mL penicillin/streptomycin.

For cell migration assays, ~500μm-wide wounds were systematically created by scratching with a sterile pipette tip throughout confluent PASMC monolayers until only 20% of the cells remained adherent to the culture dish. Plates were washed, fresh medium was added, and cells were cultured at 37°C for the indicated times.

The Smad signalling pathway was assessed by recombinant human TGF-β1 and BMP4 (R&D) and the ALK5-specific inhibitor SB525334 (Tocris Bioscience, Bristol, UK). For LXR/RXR activation studies, cells were incubated with 22R-Hydroxycholesterol (22R), or 9-*cis*-retinoic acid (9cRA) (Sigma-Aldrich, St. Louis, MO, USA). Estradiol (E2, 17β-estradiol) was used to stimulate the estrogen receptor pathway.

RNA extraction, reverse transcription and TaqMan qPCR Analysis

Total RNA from PASMCs was obtained using the miRNeasy kit (Qiagen, Hilden, Germany) following the manufacturer's instructions. cDNA for miRNA analysis was synthesized from total RNA using specific stem-loop reverse transcription primers according to the TaqMan MiRNA Assay protocol (Applied Biosystems, Foster City, CA, USA). Retrotranscription was carried out for 30

minutes at 16°C, 30 minutes at 42°C, 5 minutes at 85°C and then held at 4°C. Total cDNA for pri-miRNA and mRNA transcripts analysis was generated from total RNA using the TaqMan® Reverse Transcription Reagents (Applied Biosystems) using random hexamers. Reaction was performed for 10 minutes at 25°C, 30 minutes at 48°C, 5 minutes at 95°C.

For quantitative PCR (qPCR), 10µl reactions were incubated in a 384-well optical plate at 95°C for 10 minutes, followed by 40 cycles of 95°C for 15 seconds and 60°C for 1 minute. Data were normalized to RNU48 values for miRNAs and to B2M for pri-miRNAs expression using the $2^{-\Delta\Delta Ct}$ method. Results were expressed as fold change relative to the relevant control. The qPCRs were run in triplicate and results are presented as the mean ± standard error of samples.

Luciferase reporter activity and site-directed mutagenesis

HeLa cells were seeded in 24-well plates and then transfected with the corresponding reporter plasmid and pCMV/β-Gal vector with Lipofectamione 2000 (Invitrogen) according to the manufacturer's instructions. After 24 hours, cells were treated or not with the indicated treatment and incubated for an additional 24 hours in four replicates at least. Then, cells were washed, lysed and luciferase activity was measured with the Luciferase Assay System (Promega) in a plate reader luminometer. Data are presented as relative luciferase units (RLU) refereed to β-Galactosidase activity using the Tropix Galacton-Plus kit (Applied Biosystems), as an internal control.

Full length promoter in pGL3 (p1.5-luc) was used as the template for site-directed mutagenesis using the GENEART® Site-Directed Mutagenesis System (Invitrogen), following the manufacturer's protocol. All the primers used to specifically destroy the response elements introduced also a unique restriction enzyme site for a quick confirmation of the reaction. Their sequences are the following:

Smad3(-592)-S: 5'-GGGAGTAGCTTCCCACGCGTTGGGCTCTCCTTCCC

Smad3(-592)-AS: 5'-GGGAAGGAGAGCCCAACGCGTGGGAAGCTACTCCC

LR(-1129)-S: 5'-CCTTGATTTGTGTTTTCTGAATTCTCTTCACAGACAC

LR(-1129)-AS: 5'-GTGTCTGTGAAGAGAATTCAGAAAACACAAATCAAGG

LR(-673)-S: 5'-CCCCTGCCCTGTGGTACCCCTGCCAGGTGGCTGGG

LR(-673)-AS: 5'-CCCAGCCACCTGGCAGGGGTACCACAGGGCAGGGG

LR(-4)-S: 5'-GGTAAAAGGCAGAGTGGCAGCTGTGGCCAGGGAGCC

LR(-4)-AS: 5’-GGCTCCCTGGCCACAGCTGCCACTCTGCCTTTTACC

LR(+98)-S: 5’-GGCACCAGAGGCTGCAGCTAATTAGTTGAGAAGC

LR(+98)-AS: 5’-GCTTCTCAACTAATTAGCTGCAGCCTCTGGTGCC

ER(-801)-S: 5’-GAATCTGTAGGATCCCAAGGTGGGCTAGCAAAAGGAG

ER(-801)-AS: 5’-CTCCTTTTGCTAGCCCACCTTGGGATCCTACAGATTC

ER(-14)-S: 5’-CATATAAGGTAAAAGCTCGAGTGGCCTCTGTGG

ER(-14)-AS: 5’-CCACAGAGGCCACTCGAGCTTTTACCTTATATG

HRE(-1157)-S: 5’-GCCGAGGCCTGGTTCATATGATCCCTTGATTTGTG

HRE(-1157)-AS: 5’-CACAAATCAAGGGATCATATGAACCAGGCCTCGGC

HRE(-113)-S: 5’-GGTCAAGGCAAGGTAGTCATATGGGGGGTGCCTGGG

HRE(-113)-AS: 5’-CCCAGGCACCCCCCATATGACTACCTTGCCTTGACC

Mutations are in red and the corresponding restriction enzyme target is underlined. All these resulting mutant reporters were confirmed by sequencing.

Smad3 decoy assays

For transcription factor decoy assays, phosphorothioate oligodeoxynucleotides (PTO-ODN) were synthesized and HPLC purified (Eurofins MWG Operon, Ebersberg, Germany). The sense and antisense PTO-ODN 3’-ends were protected from nucleases by a phosphorothioate backbone (PTO). Moreover, sense ODN was 5’-FAM-labeled for visualisation after transfection. Thus, the sequence for the sense (S) and anti-sense (AS) probes was:

Mock-S: 5'-^{FAM}GGCCTCGTTTGCATGATGATgG

Mock-AS: 5’-CCATCATCATGCAAACGAGGcC

WT-S: 5’-^{FAM}CTTCCCACGGTCTGGGCTCTcC

WT-AS: 5’-GGAGAGCCCAGACCGTGGGAaG

rs12517403-S: 5’-^{FAM}CTTCCCACGGTCCGGGCTCTcC

rs12517403-AS: 5’-GGAGAGCCCGGACCGTGGGAaG

rs116423755-S: 5’-^{FAM}CTTCCCACGGTCTAGGCTCTcC

rs116423755-AS: 5’-GGAGAGCCTAGACCGTGGGAaG

Lower case letters indicate where the PTO bond is, Smad3 binding site is underlined and SNPs are in red. For probe hybridisation, sense and antisense ODN were mixed at 50 μM each, incubated at 90°C for 2 minutes and cooled at room temperature. Then, 100 pmol of double strand probes were transfected with Lipofectamine 2000 (Invitrogen) in subconfluent PASMC in 6-wells plates. Transfection efficiency was monitored by an epifluorescence microscope.

Ethical information

All animal procedures conform to the United Kingdom Animal Procedures Act (1986) and with the "Guide for the Care and Use of Laboratory Animals" published by the US National Institutes of Health (NIH publication No. 85-23, revised 1996). Animal approval was granted by the University Committee Board. Experimental procedures using human PASMCs conform to the principles outlined in the Declaration of Helsinki.

Chronic Hypoxia Mouse model

MiR-143−/− mice have previously been described 2. Homozygous miR-143−/− female mice or age-matched wild-type controls (strain C57BL6J/129SVEV, 8 weeks of age) were exposed to chronic hypoxia for 14 days or maintained in normoxic conditions and assessed at 10 weeks of age. For the reverse study, mice were exposed to chronic hypoxia for 21 days. The development of chronic hypoxic PH in mice was achieved with hypobaric hypoxia as previously described 3.

Hemodynamic Measurements

For all the experiments, right ventricular systolic pressure (RVSP) was measured in mice under isoflurane (1.5% O_2) anaesthesia via a needle advance into the right ventricle (RV) trans-diaphragmatically. Systemic arterial pressure (SAP) was recorded via a cannula placed in the carotid artery as previously described [3]. Right ventricular hypertrophy (RVH) was determined as ratio of the ventricular wall weight to the left ventricle plus septum (LV + S) weight.

Chronic Hypoxia calf model

The neonatal calf model of severe hypoxia-induced pulmonary hypertension has been described previously [4], and includes the development of pulmonary artery (PA) pressure equal to, or exceeding, systemic pressure, accompanied by remarkable PA remodelling with medial and adventitial thickening, as well as perivascular inflammation [5, 6]. Briefly, one-day-old male Holstein calves were

exposed to hypobaric hypoxia (PB=445 mmHg) for 2 weeks, while age-matched controls were kept at ambient Denver altitude (PB=640 mmHg). Standard veterinary care was used following Institutional guidelines, and procedures were approved by Colorado State University IACUC and performed at Department of Physiology, School of Veterinary Medicine, Colorado State University (Fort Collins, CO). Animals were euthanized by overdose of sodium pentobarbital (160 mg/kg body weight).

In addition to neonatal calves, older (yearling) animals with naturally-occurring pulmonary hypertension were used [7]. These animals were of mixed British-based Aberdeen Angus and Hereford breeds, they were born at a high altitude (2,438 m) cattle ranch in Southwest Colorado, and pastured at 2,438–3,505 m altitude for several months until their incidental death. Post-mortem, lung lesions consistent with PH and right-heart failure in the absence of bronchopneumonia were validated.

Western Blotting

Protein expression analysis was derived by Western blot analysis as previously described[8]. Briefly, protein was extracted from lung tissues by homogenization and protein quantified using BCA Protein Assay Reagent (Thermo Scientific). SDS-PAGE gels (NuPAGE® Novex® 10% Bis-Tris Midi Protein Gels) were calibrated with rainbow marker protein standards (Amersham). Anti-PCNA (ab18197, 1:1000), anti-FAK (phosphor Y397, ab81298 1:1000), anti- FAK (ab40794 1:1000), anti-stat3 (phopho Y705, ab76315 1:10,000) and anti-stat3 (ab68153 1:1000) were used as primary antibodies (AbCam). Primary antibodies purchased from Cell Signalling were anti-α-Tubulin (2148), AKT (C67E7) and Akt-Ser473 (5473) and these were used at 1:1000. Two secondary antibodies (peroxidase-labeled anti-mouse and anti-rabbit antibodies) were each used at a dilution of 1:2000. For protein loading control, the housekeeping protein α-Tubulin was used. Proteins were visualized using the ECL Plus Western blotting detection kit (Amersham Biosciences U.K. Ltd).

Immunohistochemistry

Mouse tissues were fixed in 4% paraformaldehyde solution at 40°C for 18 hours and embedded in paraffin. After deparaffinization with graded concentrations of histoclear and ethanol, slides were heated in 10mM pH6.0 Na Citrate for antigen retrieval. Then the sections were incubated with 20%

normal rabbit or goat serum for 30 minutes to reduce non-specific background staining. The sections were then incubated with PCNA (Abcam) or CD31 (1:20 Dianova) in 2% rabbit or goat serum in PBS or IgG control and incubated at 4℃ overnight. Sections were then incubated with Extravidin-Peroxidase LSAB reagent (Sigma E2886) or the appropriate biotinylated secondary antibody (Dako, High Wycombe, UK) diluted in 1:200 in PBS. DAB solution (Vector Labs SK-4100) was applied for 3 or 5 minutes. The nuclei were counterstained with hematoxylin for 1min; followed by dehydration of sections.

For the calves IHC staining was performed as previously described[9], with either IgG control antibodies (Vector Labs, *Burlingame, CA)*, or smooth muscle myosin heavy chains (SM-MHC)-specific rabbit polyclonal antibodies (1:2000 dilution), kindly provided by Dr. R.S. Adelstein (National Heart, Lung, and Blood Institute, NIH, Bethesda, MD). For the human lung IHC staining was performed as previously described [10], with mouse monoclonal antibody against α-smooth muscle actin (Dako, Clone 1A4, High Wycombe, UK) or isotype matched mouse IgG nonimmune control (Dako, High Wycombe, UK). For hematoxylin and eosin staining of RV, sections were incubated with hematoxylin solution (Sigma-Aldrich, Poole, UK) for 5 minutes and then rinsed in water, washed in 95% alcohol and counterstained in eosin Y solution (Sigma-Aldrich). For mouse lung immunofluorescence, after deparaffinization sections were incubated in 30% goat serum for 30 min, then with primary antibodies against CD31 (Dianova, dilution 1:20), α-sma (Sigma, dilution 1:200) and IgG-control in PBS-1%BSA overnight at 4℃. Secondary antibodies (Alexa Fluor®, dilution 1:500) were incubated for 1 hour at room temperature. Then slides were mounted in ProLong® Gold antifade reageant with Dapi (Molecular Pobes).

In situ hybridization

For the detection of miR-143 in hypoxia-exposed neonatal calves, brisket disease cattle, mouse RV and human PAH patient lung samples, 5μm sections were rehydrated with histoclear and graded concentrations of ethanol. Then slides were boiled for 10 minutes in DEPC treated 10mM sodium citrate buffer (PH6.0) for antigen retrieval and immersed in 0.2M HCL for 20 minutes. After washing three times, 0.3% triton-X was added on the slides for 10 minutes, then incubated with 10μg

proteinase K at 37℃ for 15 minutes and finally fixed with 4% PFA for 10 minutes. Following incubation with hybridization buffer (50% formamide, 4 x SSC, 2.5 x Denhadrt's solution, 2.5mg/ml salmon DNA, 0.6mg/ml yeast tRNA, 0.025% SDS and 0.1% blocking reagent) at 60°C for 1 hour slides were incubated with 40nM miR-143 or scramble miRCURY LNA^{TM} Detection probe, 5'-DIG labeled (Exiqon, Denmark) in the same buffer at 60°C overnight. After stringency washing with different concentrations of SSC buffer and blocking (1% blocking reagent in PBS and 10% FCS) anti-DIG antibody (Roche Applied Science, Indianapolis, IN, USA) was added 1:500 overnight. After washing (0.1M Tris PH 9.0) BM purple solution or NBT/BCIP solution (Roche Applied Science, Mannheim, Germany) was added to each section respectively and left at room temperature overnight. The slides were checked the next day and mounted with Vectamount AQ (Vector Labs).

Proliferation assay

Cell proliferation was measured by BrdU incorporation using Proliferation Assay Kit (Millipore BrdU Cell Proliferation Assay Kit) according to the manufacturer's instructions. Briefly, transfected and control PASMCs were seeded (1 x 10^4) in 96 well plates 24 hours and then serum starved for 48 hours in 0.2% serum containing medium. Then PDGF was added for 72 h at 20ng/ml. BrdU diluted medium was added to each well in 96 well plates after 5 h PDGF stimulation.

Microarray

Microarray analysis of PASMC and PAECs transfected with scramble or pre-miR-143. RNA quantity and quality were assessed by NanoDrop® Spectrophotometer (Thermo Scientific, Wilmington, DE, USA). RNA integrity was assessed with the Agilent 2100 bioanalyser using the RNA 6000 Nano Kit (Santa Clara, CA). The Illumina TotalPrep RNA amplification kit (Ambion) was used to generate biotinylated, amplified RNA, from 500ng input RNA, for hybridization with the Illumina arrays (Applied Biosystems Carlsbad, California). The Illumina humanHumanHT-12 v4.0 Expression BeadChips were hybridised following the manufacturer's protocol, scanned with the Illumina BeadArray Reader and read into Illumina GenomeStudio® software (version 1.1.1).

For microarray data analysis and validation, quantile normalised and background subtracted intensity values were exported from GenomeStudio® software for data processing and analysis in R

(http://www.R-project.org) in which limma statistical analysis was carried out[11], including pairwise comparisons between the 3 groups. The microarray data and experimental design was submitted online to the ArrayExpress database (www.ebi.ac.uk/arrayexpress) following MIAME guidelines. The accessions E-MTAB-3566 and E-MTAB-3567 were allocated to the PAEC and PASMC arrays respectively. To gain further biological insights into the gene expression profiling experiments, pathway analysis was performed using Ingenuity Pathway Analysis software (Ingenuity Systems, www.ingenuity.com). To account for potentially subtle changes in levels of gene expression caused by the action of miRNAs and to ensure these changes were included in the pathway analysis we used a fold change threshold of ± 1.25.

Isolation of adult mouse cardiomyocytes and heart fibroblasts

Cardiomyocytes were isolated as previously described using the cannulation of the aorta method[12]. To isolate heart fibroblasts hearts were minced in ADS buffer and serially digested (4 repeats of 25 minutes) in 310u/mg collagenase type 2 (Worthington) and pancreatin (Sigma). After every digestion, the enzyme mix was removed from the heart pieces into a falcon tube with FCS, spun down and resuspended in FCS to build up a stock of cells.

Wound Healing Assay

PASMCs or PAECs with different treatments were incubated at 37℃ in 5% CO_2 until a complete monolayer was formed. After serum starvation for 24 hours, straight scratches for each well were made with a 200ul pipette tip. The wells were then rinsed with PBS, which was replaced with regular media. Pictures were captured at 0h and 10h or 12h time points, and then the migration distances were analysed by Image J.

Transfection of PASMC cells with Cy3-labeled pre-miR-143 precursor

Pre-miR miRNA precursor (has-miR-143-3p, Ambion) was labeled with Label IT siRNA Tracker Cy3 Kit, according to the manufacture's instructions (Mirus, Madison, WI, USA). PASMC cells (1.5 x 10^5) were transfected with 100nm of Cy3 labeled pre-miR miRNA precursor using siPort (Invitrogen, ABI). The day after transfection, cells were washed with PBS, and the medium was

switched to fresh exosome-free medium. After incubation for 36 hours, the culture medium was collected and used for exosome preparation.

Co-culture experiments

Well inserts for 6 well plates with a 0.4 μm pore-sized filter were purchased from Greiner and used following the manufacturer's instructions. PASMCs (1.5×10^5) in the well inserts with pre-miR143 (100nM) transfection by siPORT (Invitrogen) according to the manufacturer's instructions simultaneously and cultured in complete SMC medium for 24h. PAECs (2×10^5) were seeded into the 6-well plate with EBM medium. Before starting the co-culture experiments both PASMCs and PAECs were washed with PBS then the insert with transfected PASMC was put into the 6-well plate with PAECs. All co-culture experiments were done in complete EBM.

Isolation of exosomes from cell media

Cell media from PASMCs with different treatments were centrifuged at 2000g for 30 min to remove cell debris. The supernatant containing the cell free cell media was transferred to a clean tube and held on ice until use. Then each sample was combined with total exosome isolation reagent (Invitrogen) and mixed well by vortexing until a homogenous solution was formed. The samples were incubated at 4°C overnight and then centrifuged at 4 °C at 10000 g for 1 h. The supernatant was aspirated and discarded, and the exosome pellet was resuspended in PBS buffer, then stored at 4°C for short term (1-7 d) and -20 °C for long term until use. Nanosight™ and protein analysis by western blot for CD63 (H-193: sc-15363) and CD9 (H-110: sc-9148) were carried out to test the purity of the exosome isolation.

DNA Damage

PASMC were treated with TNF-α (100ng/ml), IL-6 (100nm) and PDGF (30ng/ml) for 48 hours as previous study[13]. Immunofluorescence for γ-H2AX was performed as previously reported[14] using a monoclonal antibody directed against γ-H2AX (ab11174, Abcam).

Apoptosis Assay

Pre-miR143/Scramble transfected PASMCs and PAECs and PAECS treated with miR-143 enriched exosomes derived from PASMCs were seeded in 96-well plates. After 24 hours of transfection,

PASMCs were treated with H_2O_2 (50μm) for 12 hours and PAECs were treated with Cycloheximide (CHX, 25ng/ml) and TNF-α (4ng/ml) for 7 hours. The standard protocol for cells cultured in a 96-well plate of Caspase-Glo® 3/7 Assay (Promega, G8091) was followed according to the manufacturer's protocol.

***In Vitro* Angiogenesis**

Evaluation of tube formation by PAECs was performed using an *In Vitro* Angiogensis Assay Kit (ECM625; Mliiipore, Billerica, CA). PAECs transfected with pre-miR143/Scramble or treated with miR-143 enriched exosomes derived from PASMCs were cultured on ECMatrix, a solid gel consisting of basement membrane proteins, growth factors, and proteolytic enzymes. Briefly, ECMatrix gel solution was thawed, mixed with diluent buffer, and 50μl was transferred to each well of a pre-cooled 96-well tissue culture plate. This was incubated at 37°C for 1.5 hours to allow the matrix solution to solidify. Treated PAECs were harvested, resuspended in media, seeded 1 x 10^4 cell/well onto the surface of the polymerized ECMatrix™ and incubated at 37°C for 6-12 hours. The extent of proangiogenesis was quantified by measuring the total tube length in 5 randomly selected fields (x 100 magnification) for each well. Experiments were conducted in triplicate.

Statistical analysis

All statistical calculations were carried out using GraphPad Prism. Student's *t*-tests were used when comparing two conditions and a one-way ANOVA with Bonferroni and Tukey correction was used for multiple comparisons. Probability values of less than 0.05 were considered significant.

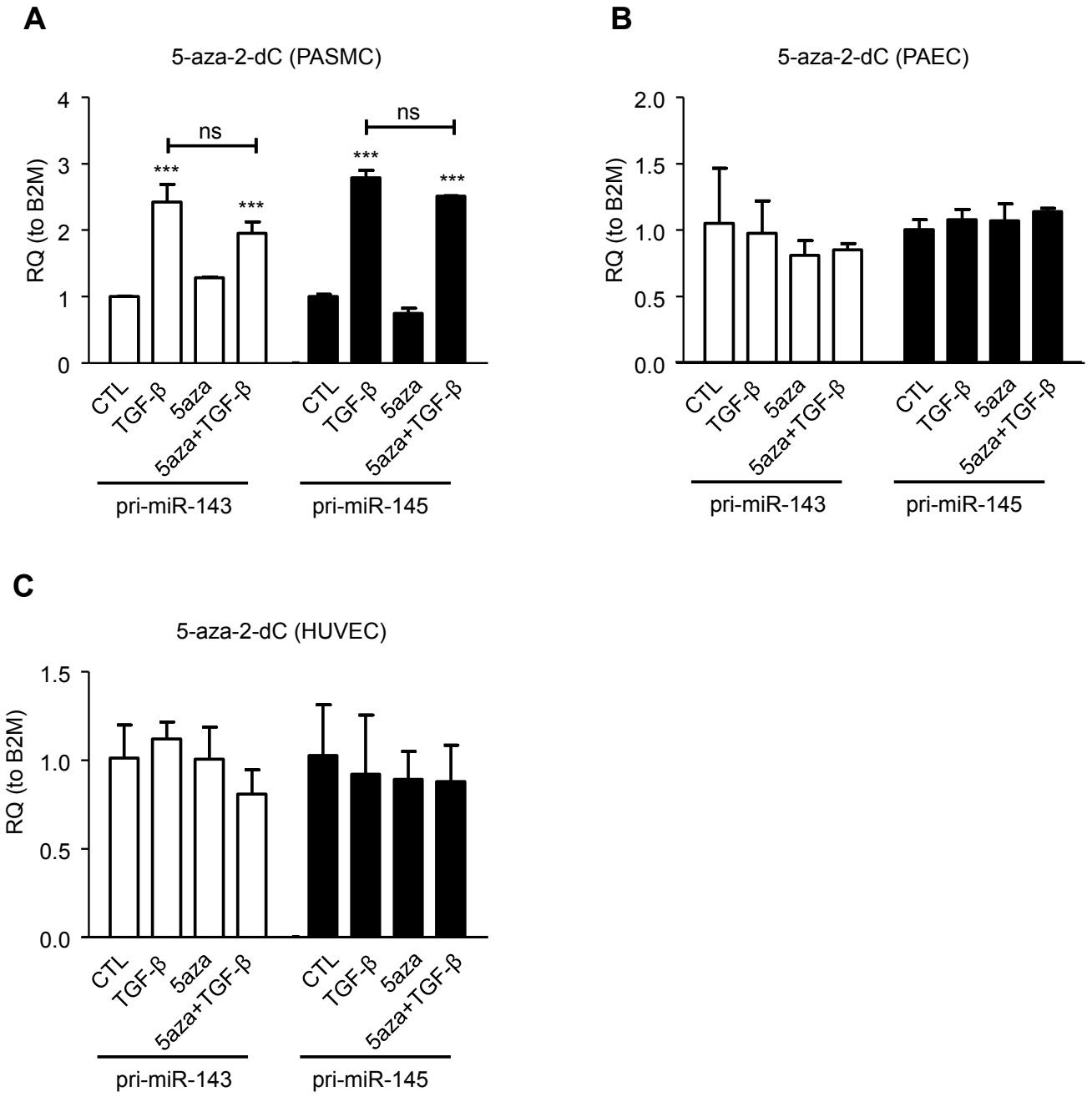

Online Figure I

Online Figure I. Analysis of the effect of methylation on pri-miR-143 expression. Human pulmonary artery smooth muscle cells (PASMC) **(A)**, pulmonary artery endothelial cells (PAEC) **(B)** and umbilical vein endothelial cells (HUVEC) **(C)** were treated with the demethylating agent 5-aza-2'-deoxycytidine (5aza) for 24 hours and with or without TGF-β for an additional 24 hours. Expression levels of pri-miR-143 and pri-miR-145 were detected by qPCR. ***p<0.001 and ns, not significant. ***p<0.005.

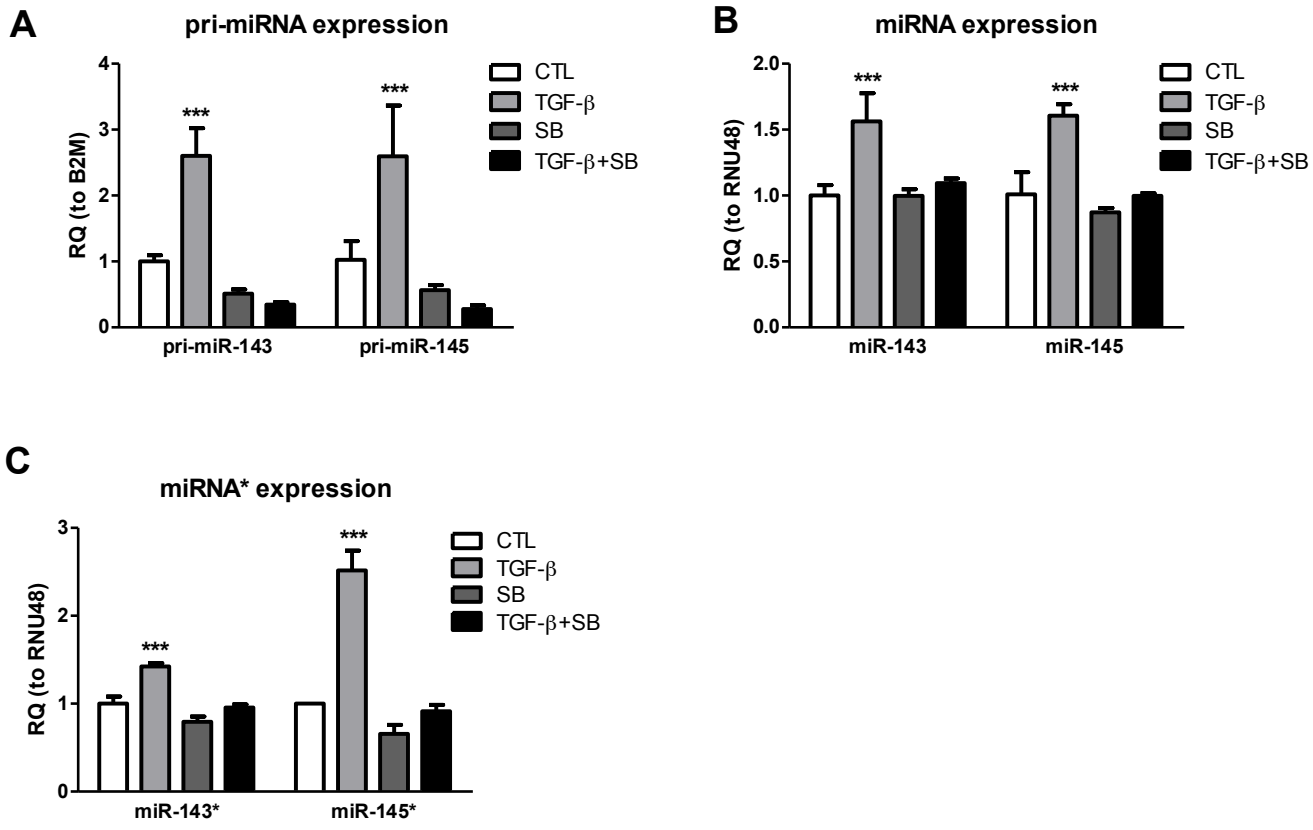

Online Figure II

Online Figure II. The effect of TGFβ on miR-143 and miR-145 expression. PASMC were treated with or without 10 ng/ml TGF-β in 0.2% FCS medium for 24 hours. In addition, cells were pre-treated with the TGF-β/ALK5-specific inhibitor SB525334 at 1 nM for 30 minutes as indicated. Pri-miR-143 and pri-miR-145 precursors **(A)**, mature lead strands miR-143-3p and miR-145-5p **(B)**, and corresponding passenger strands miR-143-5p (miR-143*) and miR-145-3p (miR-145*) **(C)** were detected by qPCR. *** $p<0.001$.

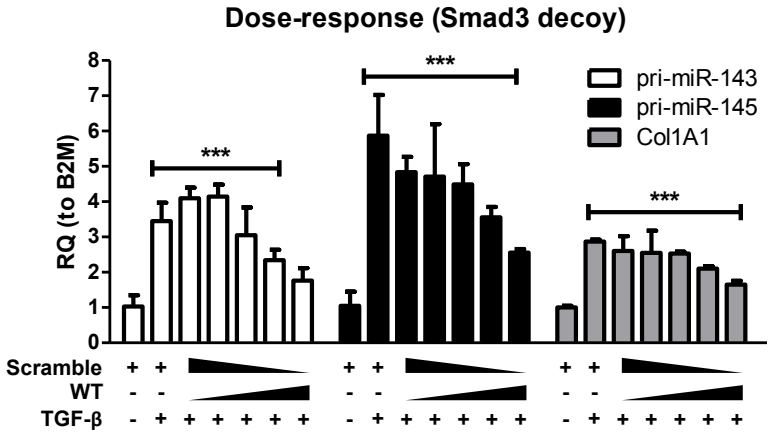

Online Figure III

Online Figure III. Expression of pri-miR-143 and pri-miR-145 in response to a dose response to Smad3 decoy probes. Increasing amounts of WT decoy probe were transfected into PASMC. Total amount of decoy probe was corrected with a scramble sequence (mock). After 6 hours post-tranfection, cells were treated with or without 10 ng/ml TGF-β for additional 24 hours. Pri-miR-143 and pri-miR-145 were detected by qPCR. Expression of α1 chain of type I collagen (COL1A1) was used as a TGF-β responsive control gene. ***p<0.001.

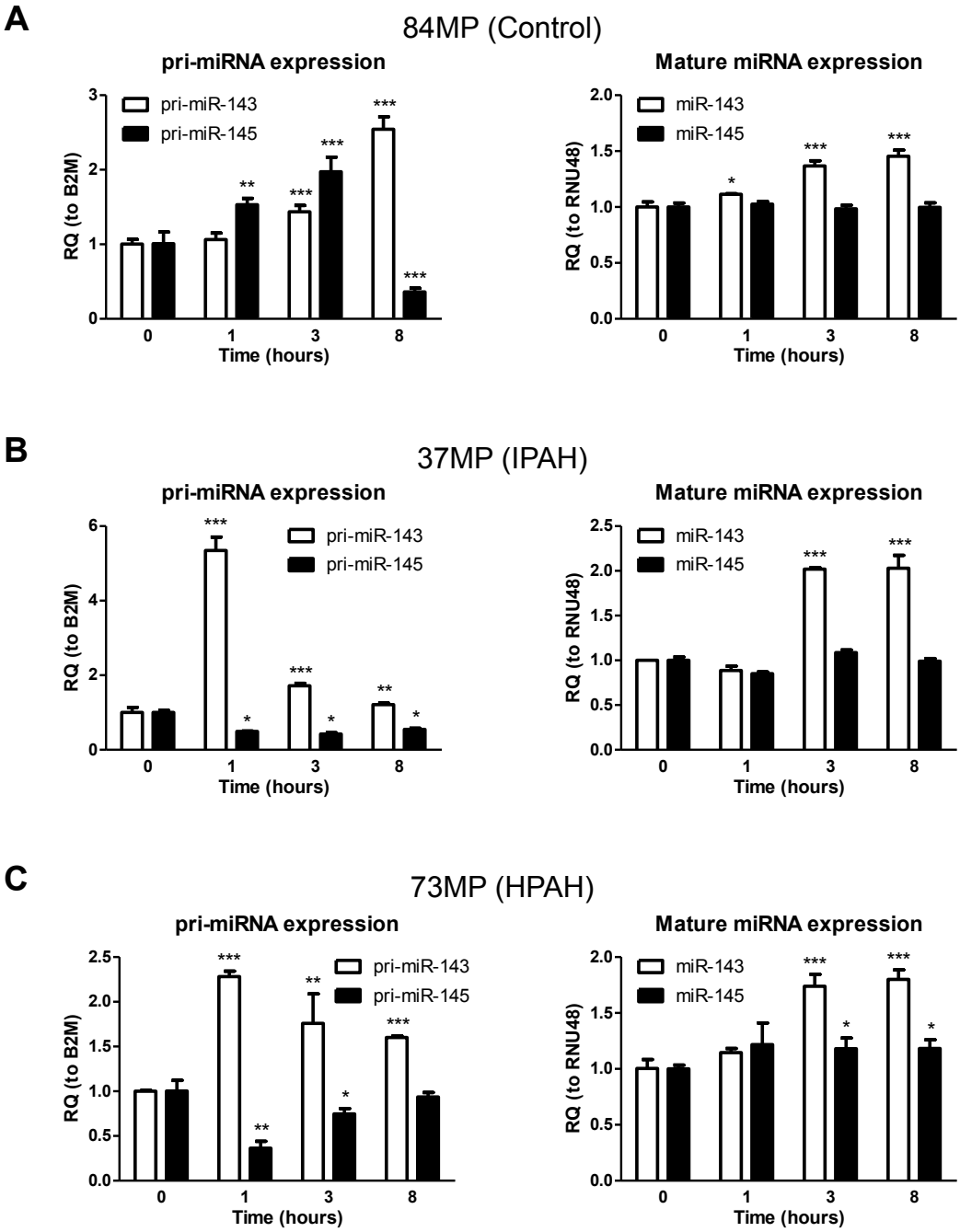

Online Figure IV

Online Figure IV. Comparative analysis of PASMC migration in control and PAH donor cells. Cells were grown in monolayer and the expression levels of miR-143 and miR-145 precursors and mature forms were detected by TaqMan qPCR at the indicated time after the scratch in control PASMC (84MP) (A). In parallel, PASMC from either idiopatic or hereditable PAH patients, 37MP (IPAH) (B) and 73MP (HPAH) (C) respectively, were also assayed. *$p<0.05$. **$p<0.01$. ***$p<0.001$.

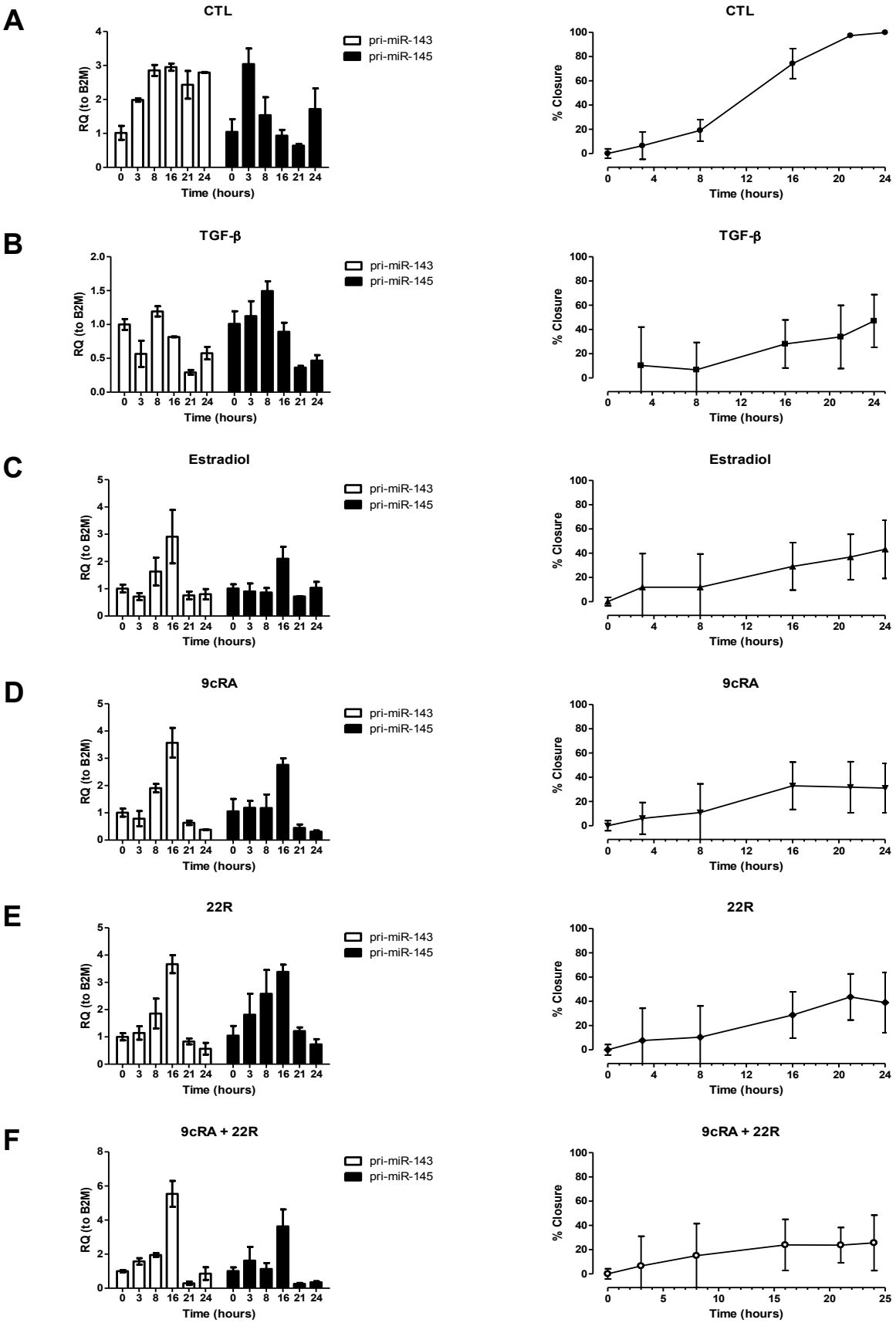

Online Figure V

Online Figure V. Cell migration in response to transcriptional regulators of miR-143. PASMC monolayers were scratched and then incubated for 0, 3, 8, 16, 21 and 24 hours with the indicated treatment **(A)**, Control with vehicle; **(B)**, 10 ng/ml TGF-β; **(C)**, 10 nM Estradiol; **(D)**, 5 μM 9cRA; **(E)**, 5 μM 22R-Hydroxycholesterol; **(F)**, 5 μM 9cRA and 5 μM 22R-Hydroxycholesterol). Left panels show expression levels of pri-miR-143 and pri-miR-145 detected by qPCR, whereas right panels show cell migration during scratch closure at the same time points. Data are represented as mean ± SD.

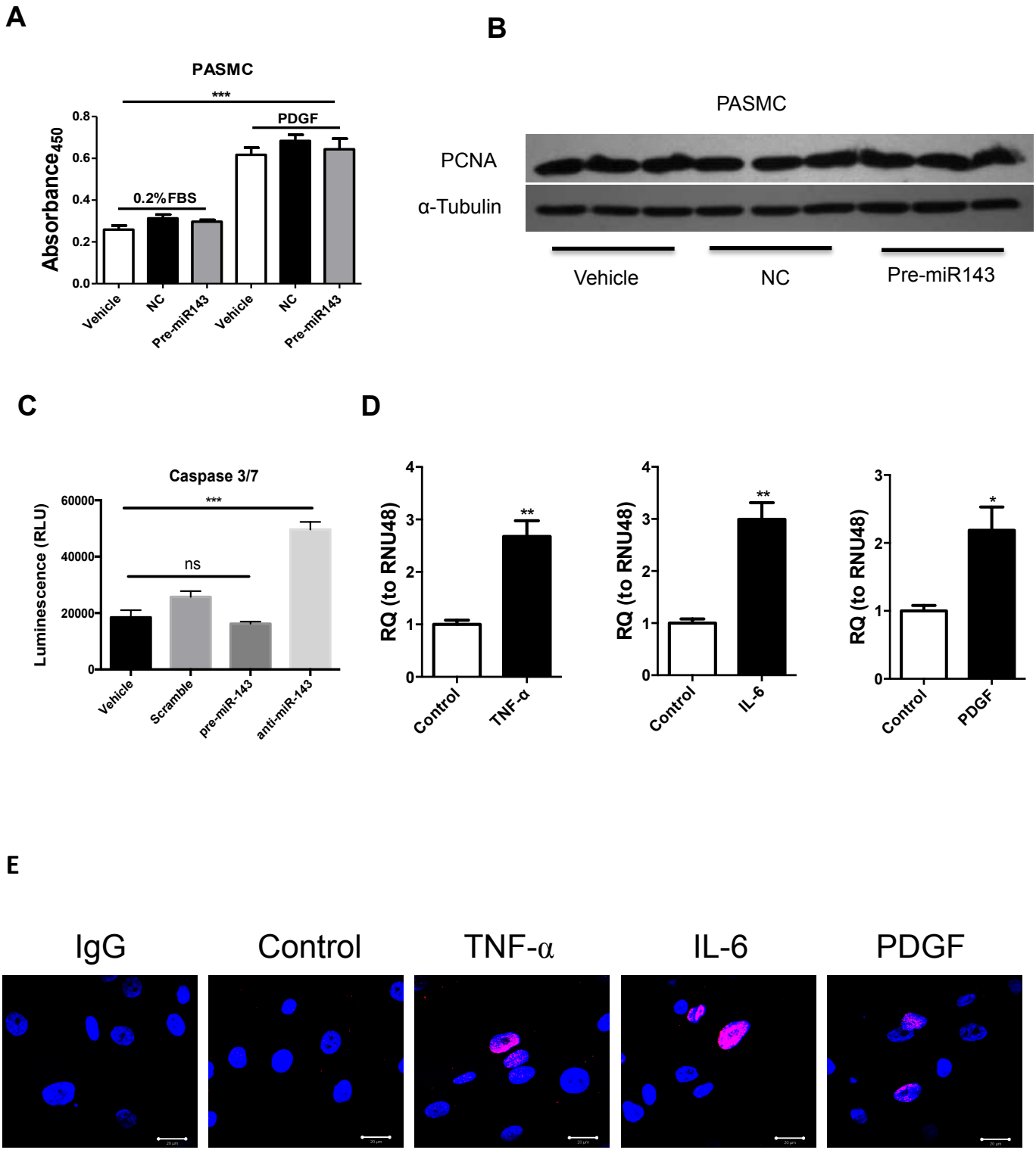

Online Figure VI

Online Figure VI. Proliferation and apoptosis of PASMCs in response to modulation of miR-143 levels. (A), Human PASMCs were transfected with pre-miR143 or negative control and pulsed with BrdU 6 hours after 20 ng/ml PDGF stimulation for 72 hours. BrdU incorporation did not change in miR-143 groups compared with NC (n=6). **(B)**, Expression of the proliferation marker PCNA was quantified in PASMCs 72 hours after transfection with pre-miR143 or negative control. Immunoblotting revealed no differences upon miR-143 transfection (n=3). **(C)**, PASMC apoptosis with pre-miR-143 and anti-miR-143 transfection were measured by caspase 3/7 activity (n=8). **(D**), Q-PCR assess the miR-143 in PASMC with TNF-α (100ng/ml), IL-6 (100nm) and PDGF (30ng/ml) treatment for 48 hours. **(E)**, Y-H2AX nuclear staining shown the PASMC DNA damage induced by TNF-α, IL-6 and PDGF. (n=3) Scale bar=20μm *$p<0.05$, **$p<0.01$, ***$p<0.001$.

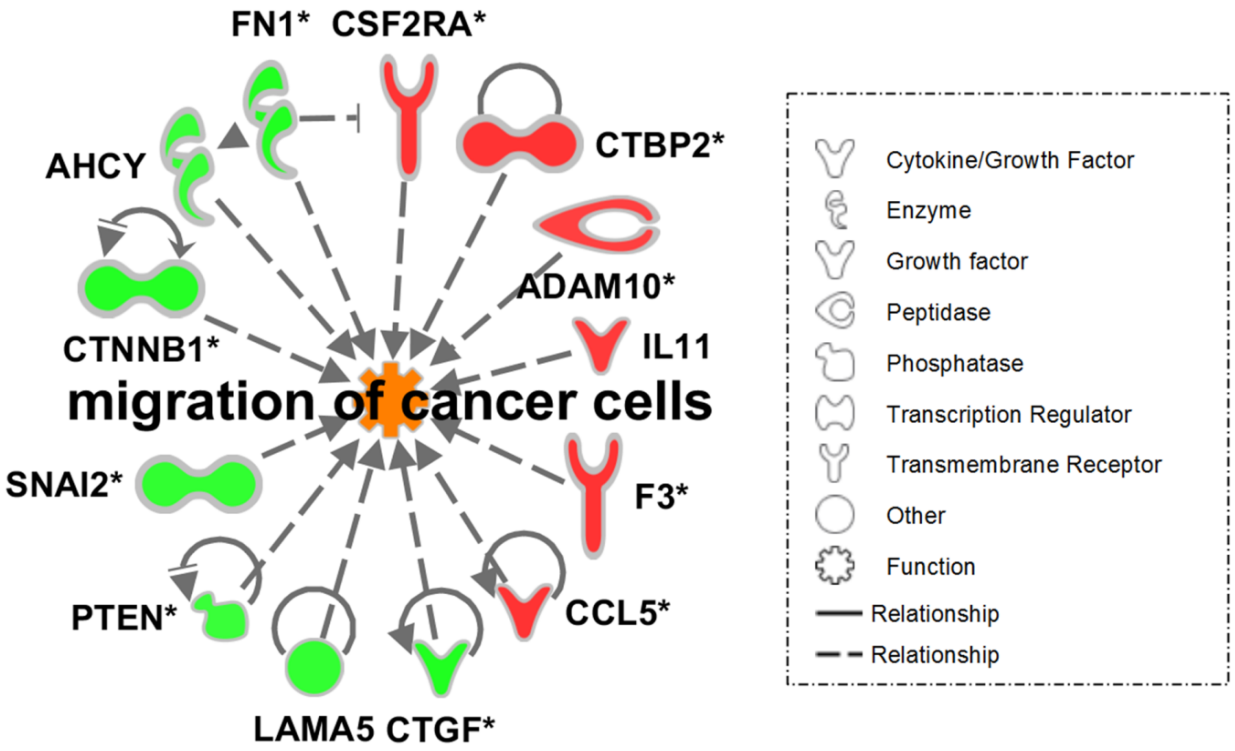

Online Figure VII

Online Figure VII. Pathway analysis by microarray. Selected significant functional annotation relating to increased 'migration of cancer cells' ($p < 1.43x10^{-4}$) using Ingenuity Pathway Analysis. Orange represents an increase in migration of cancer cells, green fill represents decrease and red an increase in gene expression levels in mir-143 transfected cells compared to controls.

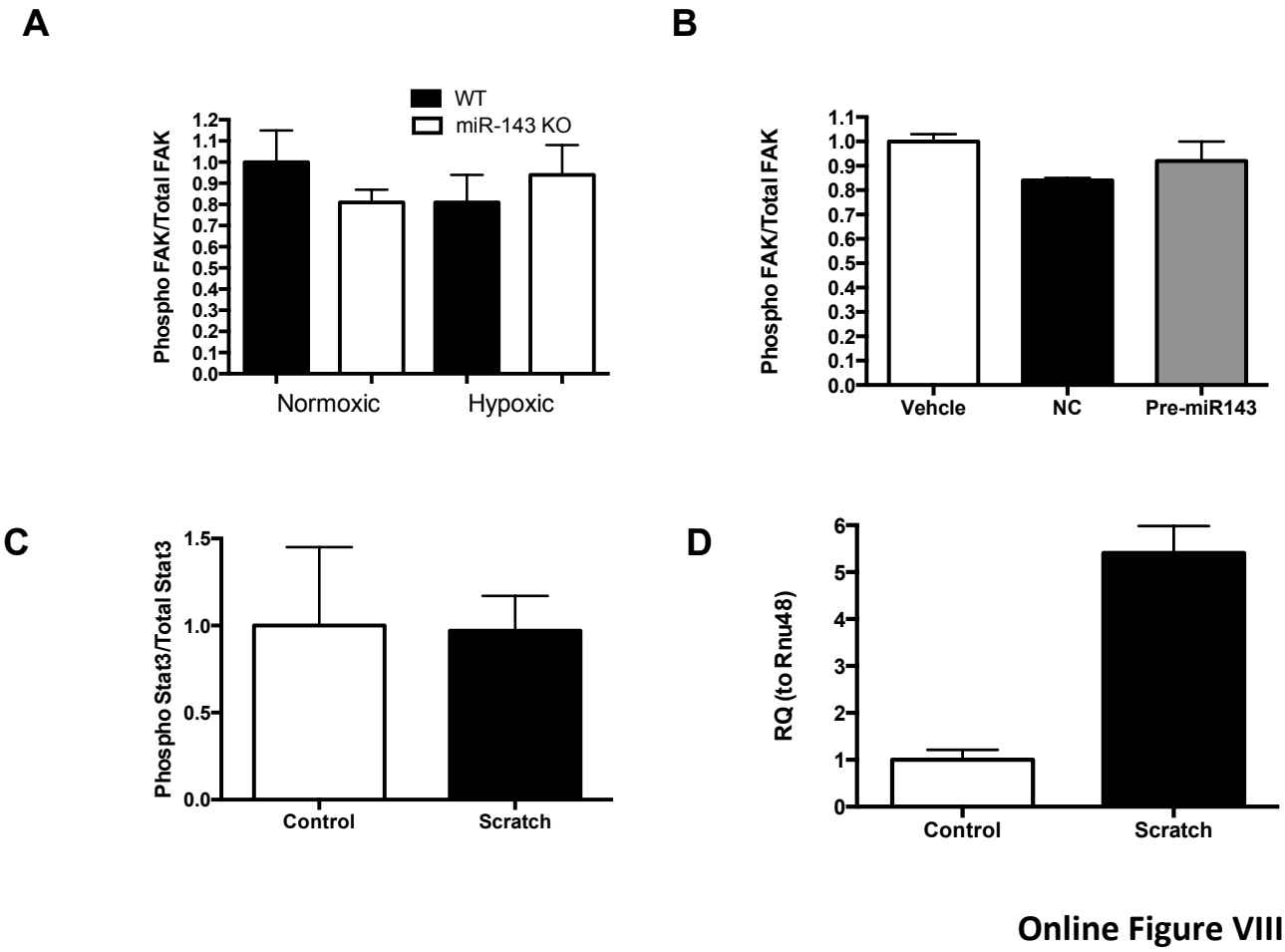

Online Figure VIII

Online Figure VIII. Western blot analysis for potential mediators of the PAH phenotype. (A), FAK phosphorylation was assessed in wild type (WT) and miR-143 knock out (miR-143 KO) lungs from mice exposed to normoxic or hypoxic conditions. Results were normalized by densitometry to total FAK (n=3). **(B)**, FAK phosphorylation was assessed in PASMCs transfected with scramble or premiR-143. Data were analysed using a two-way ANOVA n=3. **(C)**, Stat 3 (phospho Y705) phosphorylation was assessed in both control PASMCs and PASMCs 24hrs after multiple scratches (migrating) by western blot. Total stat 3 was used as an endogenous control. Results were normalized by densitometry to total stat3 (n=6). **(D)**, The expression level of miR-143 was assessed by q-PCR in control and migrating PASMCs.

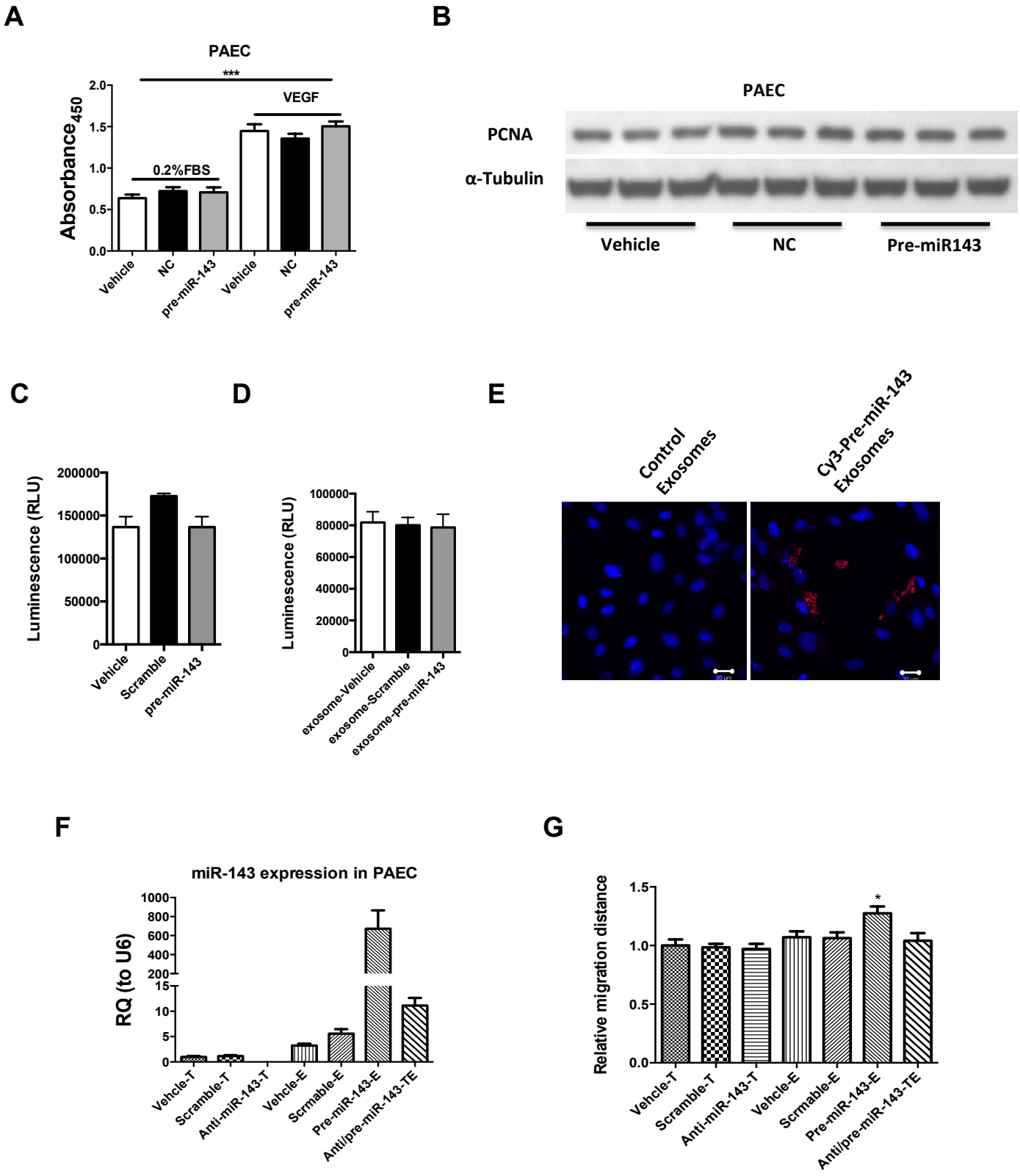

Online Figure IX

Online Figure IX. Proliferation and apoptosis of PAECs in response to modulation of miR-143 levels, and antimiR-143 transfection inhibited the miR-143-enriched exosome mediated PAEC migration. (A), Human PASMCs were transfected with pre-miR143 or negative control and pulsed with BrdU 6 hours after 20 ng/ml PDGF stimulation for 72 hours. BrdU incorporation did not change in miR-143 groups compared with NC (n=6). **(B)**, Expression of the proliferation marker PCNA was quantified in PASMCs 72 hours after transfection with pre-miR143 or negative control. Immunoblotting revealed no differences upon miR-143 transfection (n=3). **(C)**, PAEC apoptosis with pre-miR-143 transfection or **(D)** miR-143 enriched exosomes derived from PASMCs were measured by Caspase 3/7 activity (n=8). **(E)**, PAECs exposure to exosome derived from PASMC transfected with Cy3 labeled pre-miR-143 and assess the red fluorescence by fluorescent microscope. Control exosomes as negative control. Scale bar= 20μm (n=3). **(F)**, miR-143 expression in PAEC with exosomes exposure, antimiR-143 transfection alone and miR-143-enriched exosomes derived from PASMC together with antimiR-143 transfection. **(G)**, Relative migration distance in PAEC showed that the miR-143 enriched exosomes derived from PASMCs exposure induced migration could be inhibited by antimiR-143 transfection. (n=3). *$p < 0.05$, ***$p<0.001$.

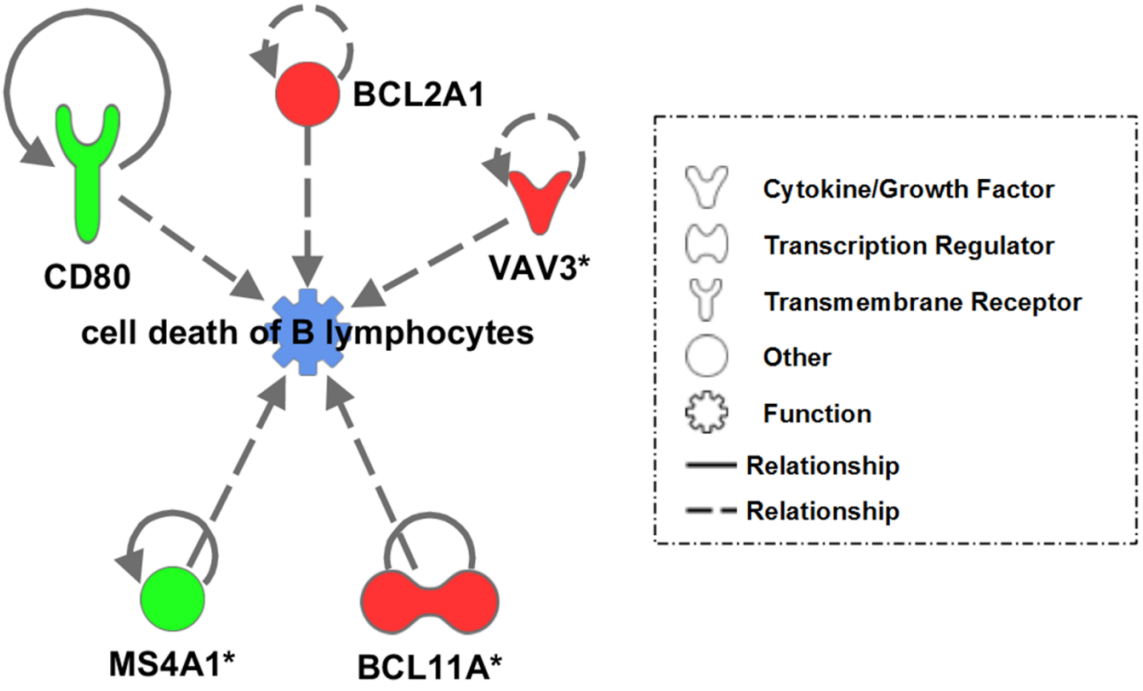

Online Figure X

Online Figure X. Pathway analysis by microarray. Selected significant functional annotation relating to decrease in 'cell death and survival' ($p < 1.56 \times 10^{-3}$) using Ingenuity Pathway Analysis. Blue represents an decrease in 'cell death of B lymphocytes', green fill represents decrease and red an increase in gene expression levels in mir-143 transfected cells compared to controls.

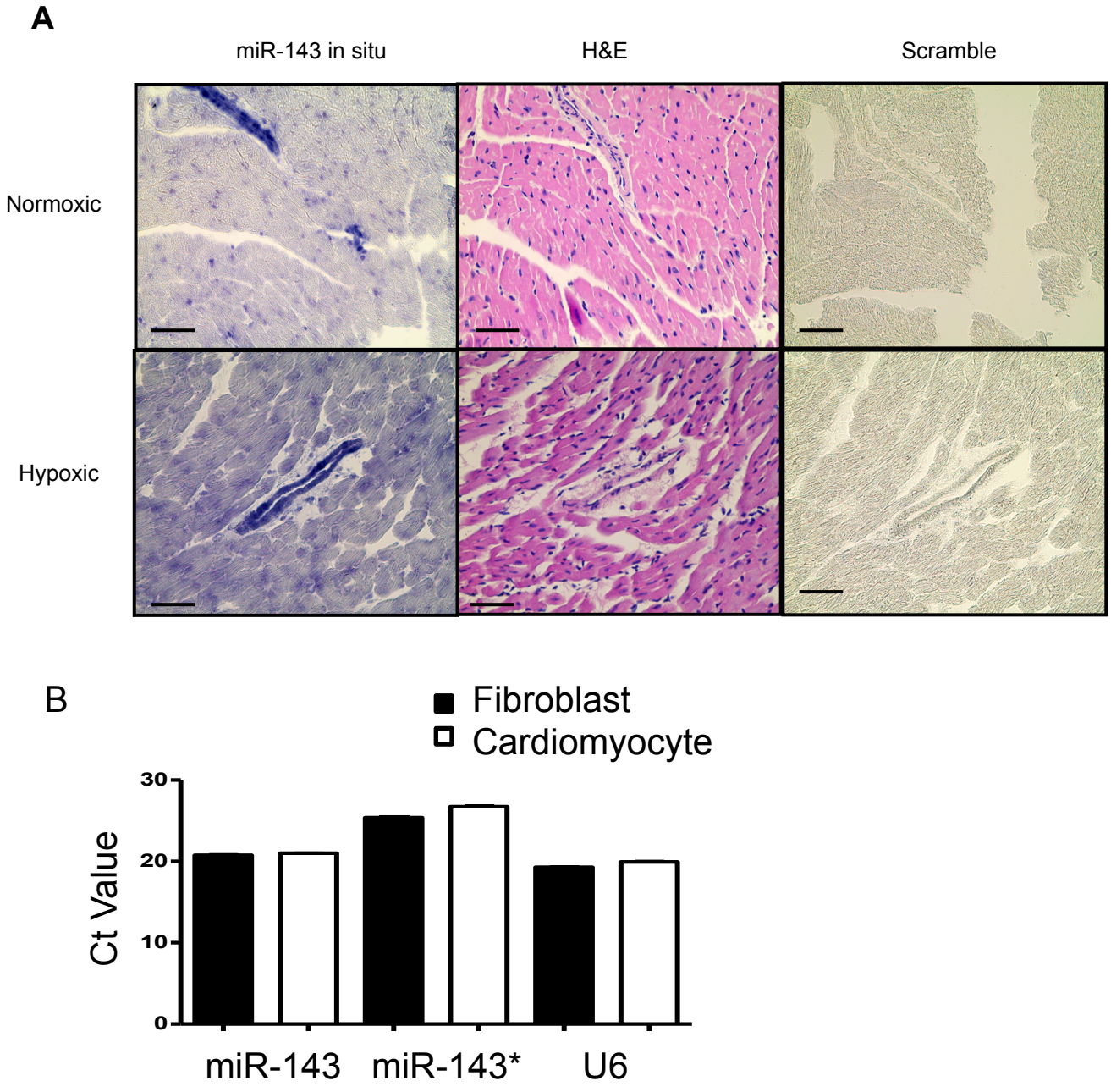

Online Figure XI

Online Figure XI. In situ hybridization showing miR-143 localisation in RV from mice exposed to normoxic or hypoxic conditions and miR-143 expression in Fibroblast and Cardiomyocytes. (A), Paraffin sections were rehydrated and incubated with an anti–miR-143 or scramble probe as negative control. Hematoxylin and eosin (H&E) stains were used to identify cardiomyocytes. Images ×40 magnification, bar represents 50μm (n=5). **(B)**, The expression level of miR-143 and miR-143* was assessed by q-PCR in cardiac fibroblasts and cardiomyocytes.

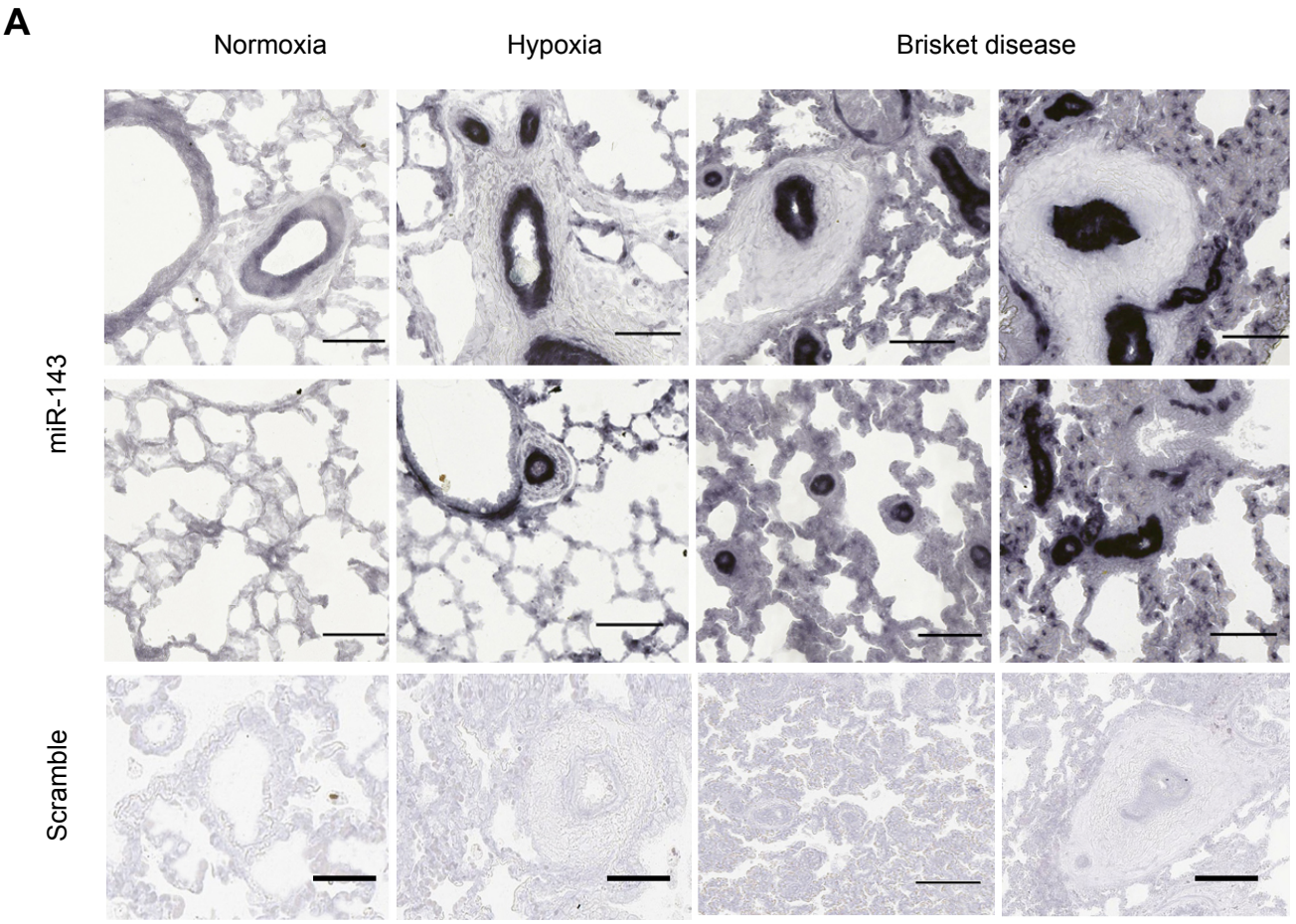

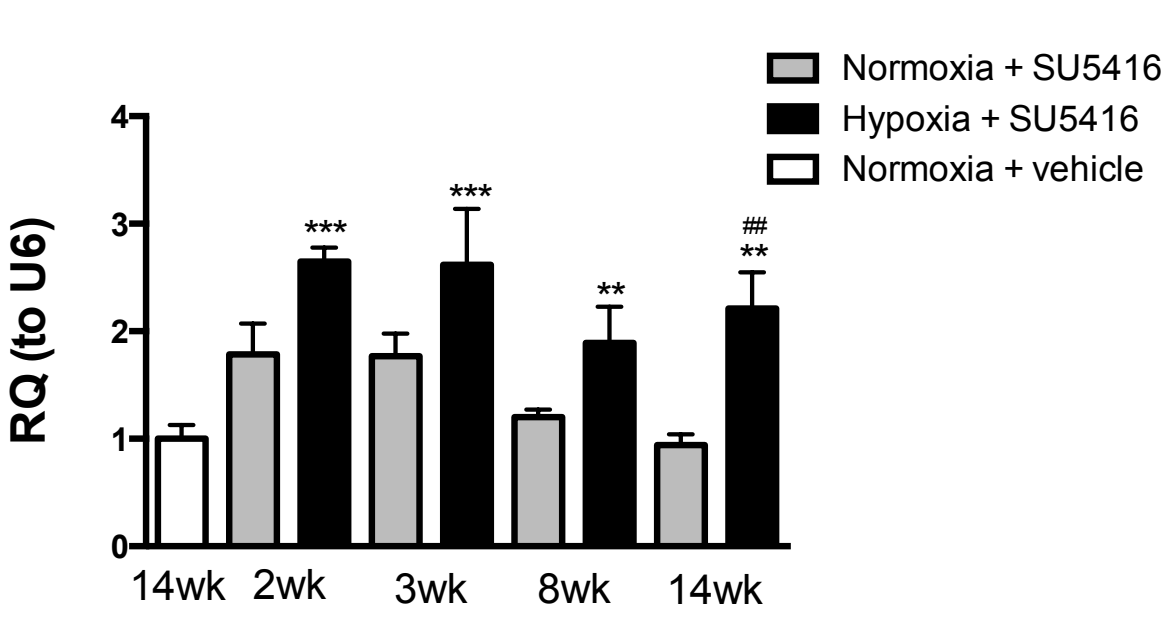

Online Figure XII

Online Figure XII. In situ hybridization analysis of miR-143 expression in paraffin sections obtained from Brisket disease and control calves and miR-143 expression in different stages of rat SUGEN model. (A), A scramble probe was used as negative control. MiR-143 expression in distal pulmonary arteries was significantly upregulated in Brisket disease compared with controls. Images all x40 magnification, scale bars = 100μm. **(B)**, miR-143 detected by qRT-PCR in lung from male rats exposed to normoxic or hypoxic conditions for 2 wks coupled with subcutaneous administration of 20 mg/kg SU5416 on day 0, followed by varying lengths of time in normoxic conditions. Total study time indicated on x-axis. Arbitrary value of 1 assigned to 14 wk normoxia + vehicle. Data represented as fold change ± SEM and analysed by a one-way ANOVA followed by Tukey's post hoc test, n = 5 animals per group. *$p<0.05$, **$p<0.01$, ***$p<0.001$ vs 14 wk normoxia + vehicle, ##$p<0.01$ vs time matched normoxia + SU5416.

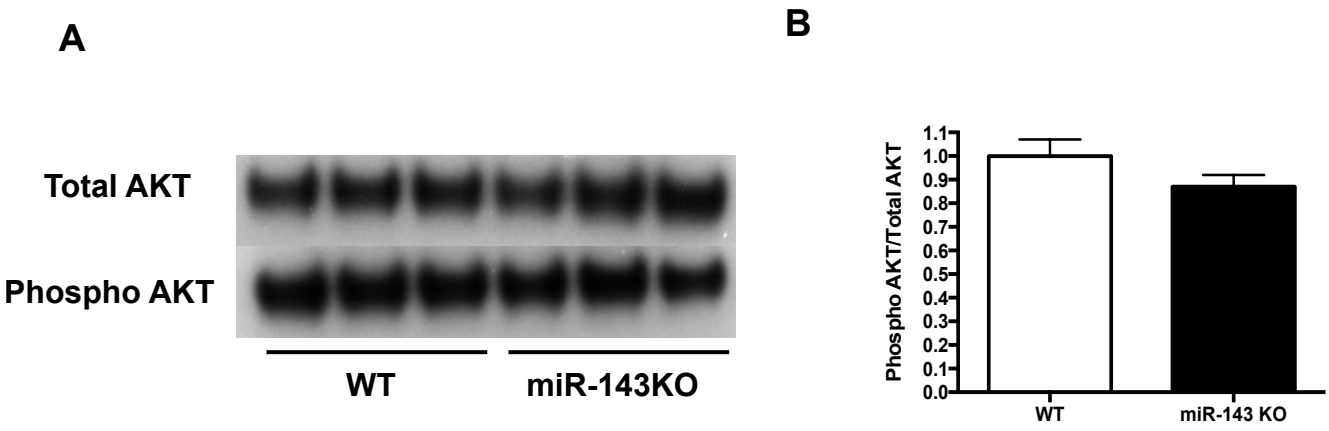

Online Figure XIII

Online Figure XIII. Assessment of AKT. (A), AKT phosphorylation (phospho Ser473) was analysed by Western blot in WT and miR-143KO RV from mice. **(B)**, AKT phosphorylation was normalized by densitometry to total AKT. Data were analysed using a t-test (n=6). For all data an arbitrary value of 1 was assigned to the control group.

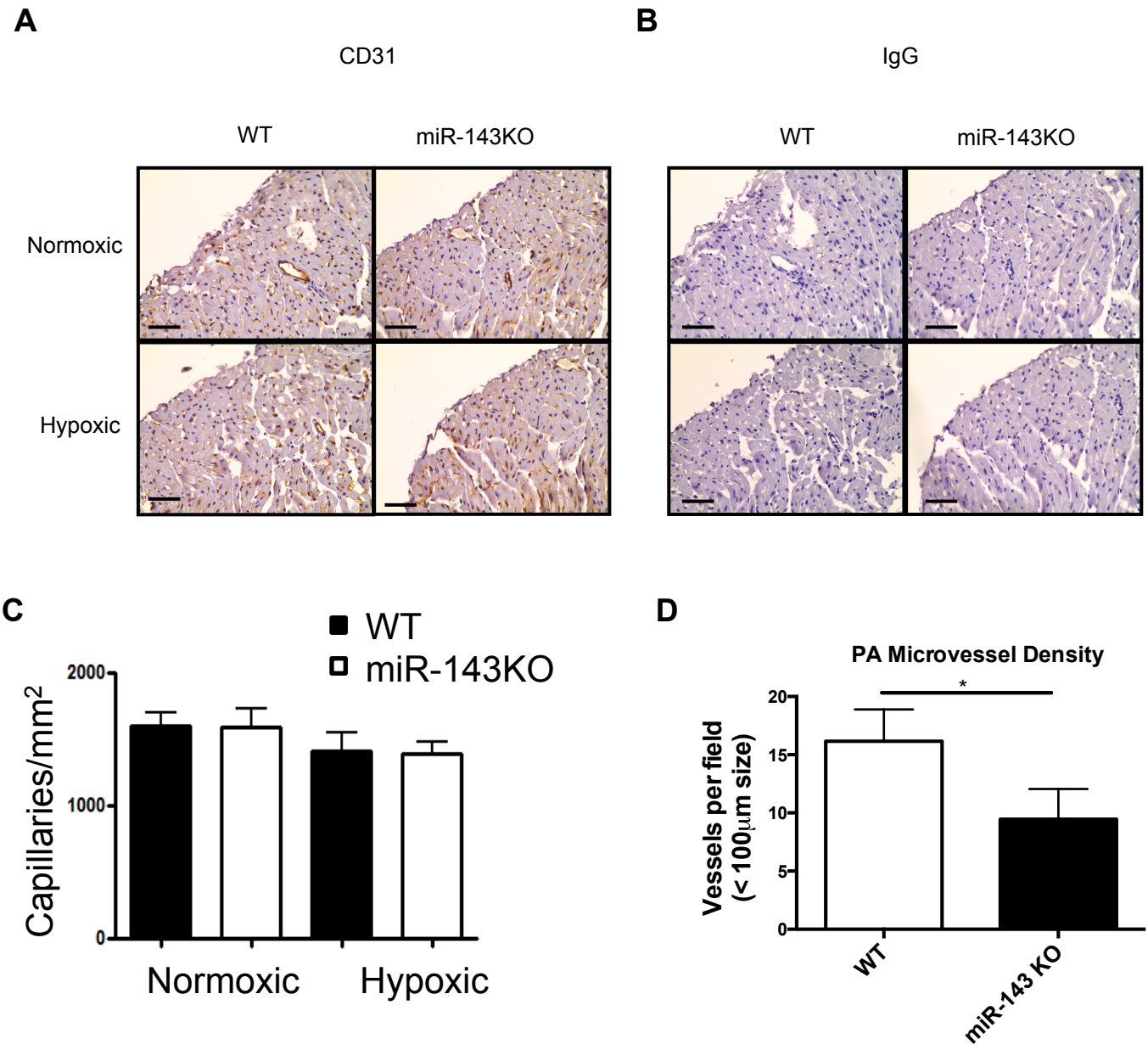

Online Figure XIV

Online Figure XIV. Histological sections of the right ventricles and total lung from wild type and miR-143 knock out (miR-143KO) mice, stained for RV capilarisation. CD31 staining **(A)** and IgG control **(B)** were performed and microvessel density was quantified **(C)**. Images ×40 magnification, scale bar represents 50μm (n=5). **(D),** microvessel density was quantified in the total lung sections of miR-143$^{-/-}$ and WT hypoxia mice by CD31 and α-SMA staining (n=4). *$p < 0.05$.

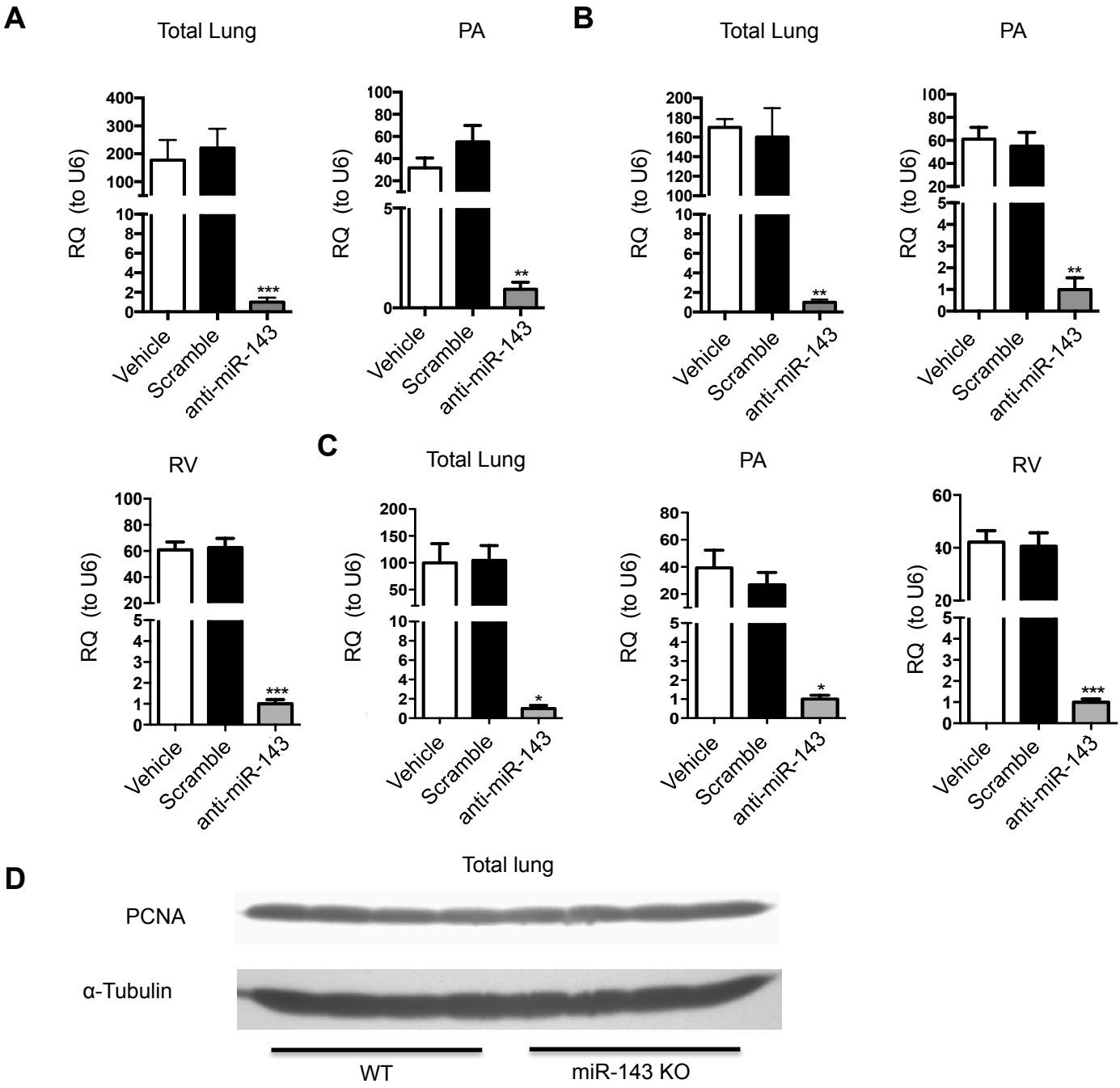

Online Figure XV

Online Figure XV. Validation of the antimiR-143 study and analysis of PCNA. **(A)**, Q-PCR confirmed the miR-143 knockdown in total lung and pulmonary arteries (PA) with antimiR-143 injection in normoxia in vivo (n=8). **(B)** and **(C)**, Q-PCR confirmed the miR-143 knockdown in total lung, pulmonary arteries (PA) and right ventricles (RV) of prevention and reversal PH model with antimiR-143 injection under chronic hypoxia conditions in vivo (n=8). **(D)**, Expression of the proliferation marker PCNA was quantified in the total lung protein of WT and miR-143 KO chronic hypoxia mice (n=4). **(E)**, Immunohistochemical analysis showed there was no difference of PCNA expression on the pulmonary arteries of WT and miR-143 KO chronic hypoxia mice (n=4). *$p < 0.05$, **$p < 0.01$ and ***$p<0.005$.

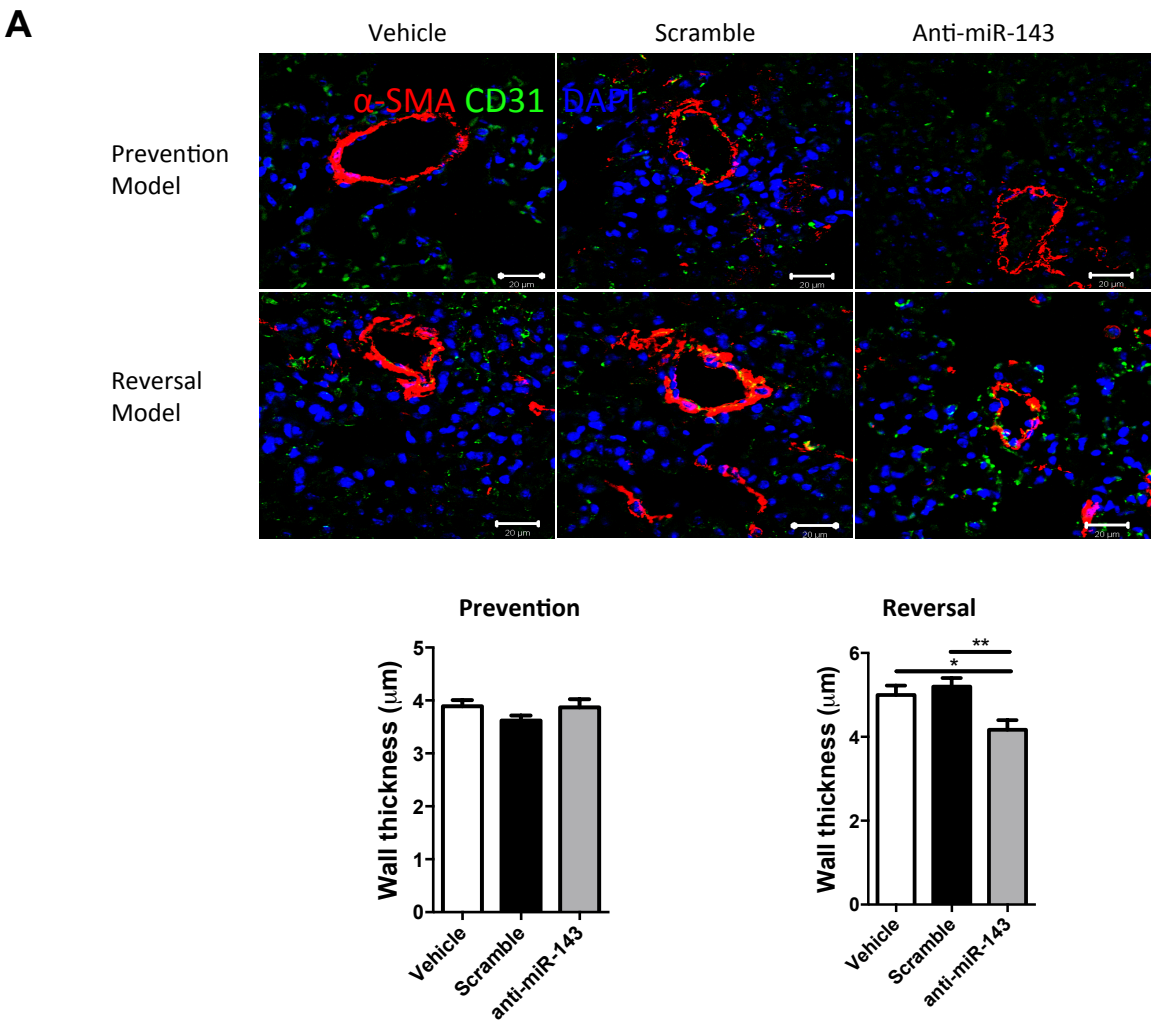

Online Figure XVI

Online Figure XVI. Vascular remodeling of the miR-143 pharmacological inhibition PH mice models. (A), Distal pulmonary artery vessel wall thickness and remodeling were analyzed by α-smooth muscle actin (α-SMC) and CD31 staining in both prevention and reversal PH model by anti-miR-143 injection compared with control groups (n=5, scale bar=20μm). *p < 0.05, **p < 0.01

Supplemental Tables

Supplementary Table I. Disease and function annotation relating to migration in the smooth muscle cell gene expression dataset.

Categories	Diseases or Functions Annotation	p-Value	Gene Count	Molecules
Cellular Movement	migration of brain cells	5.53E-05	9	APP,BTG2,CDK5,FN1,FUT10,GNA13,LAMA1,PTEN,RERE
	migration of breast cancer cell lines	2.96E-03	12	ANKS1A,CCL5,CTGF,CTNNB1,CTSL,DDR2,FLNA,FN1,GIT1,MLLT4,SNAI2,TGM2
	migration of cancer cells	1.43E-04	13	ADAM10,AHCY,CCL5,CSF2RA,CTBP2,CTGF,CTNNB1,F3,FN1,IL11,LAMA5,PTEN,SNAI2
	migration of cells	3.64E-04	68	ADAM10,ADORA1,AHCY,ANGPTL4,ANKS1A,APP,ARHGDIA,ASAP2,BBS1,BTG2,CCL5,CCR5,CD58,CD63,CDK5,CSF2RA,CTBP1,CTBP2,CTGF,CTNNA1,CTNNB1,CTSL,DDR2,DIAPH1,DOCK3,F3,FCAR,FLNA,FN1,FUT10,FUT8,GIT1,GNA13,GNG12,HDAC3,HDC,HLA-G,HRH1,IL11,JAK1,LAMA1,LAMA5,LDLR,LPA,MATN2,MLLT4,MYOCD,PKD1,PKM,PLEC,PRRX1,PTEN,PTPRU,RERE,RHOG,SCARB1,SEMA3E,SLC3A2,SLC9A1,SNAI2,SPRY4,TGM2,TP53INP1,TPT1,TRPV1,WHSC1,YWHAE,YY1AP1
	migration of central nervous system cells	2.37E-05	10	APP,BTG2,CDK5,CTGF,FN1,FUT10,GNA13,LAMA1,PTEN,RERE
	migration of chondrosarcoma cells	1.03E-02	2	CCL5,IL11
	migration of embryonic cells	3.08E-03	7	CCL5,CDK5,FN1,IL11,LAMA1,LAMA5,SLC3A2
	migration of endothelial cells	9.72E-03	14	ADAM10,ANGPTL4,CCL5,CD63,CTGF,F3,FLNA,FN1,HRH1,PKM,PTEN,SCARB1,SEMA3E,SPRY4
	migration of extravillous trophoblast cells	3.00E-03	2	CCL5,IL11
	migration of fibroblast cells	3.48E-03	8	CTNNB1,FN1,GNG12,PKD1,PTEN,RHOG,TGM2,TP53INP1
	migration of glioma cells	9.43E-03	3	CSF2RA,CTGF,F3
	migration of hepatic stellate cells	6.56E-03	3	CCL5,CCR5,CTGF
	migration of kidney cell lines	1.57E-03	7	ANKS1A,APP,CCL5,CCR5,FN1,PKD1,RHOG
	migration of leukemia cells	5.33E-04	7	APP,CCL5,CCR5,FLNA,FN1,GNA13,TGM2
	migration of melanoma cells	8.41E-03	3	ADAM10,FN1,SNAI2
	migration of monocytes	6.45E-03	6	APP,CCL5,CTGF,FN1,JAK1,LDLR
	migration of mononuclear leukocytes	6.50E-03	16	ADAM10,APP,CCL5,CCR5,CD58,CTGF,DIAPH1,FN1,GNA13,HDC,HLA-G,JAK1,LDLR,PLEC,PTEN,TGM2
		2.12E-03	3	APP,BTG2,FUT10

	migration of neural precursor cells			
	migration of neuroglia	9.97E-03	5	APP,CTGF,FN1,MATN2,PTEN
	migration of neurons	2.06E-03	13	ADAM10,BBS1,CDK5,CTNNB1,DIAPH1,FLNA,FN1,GNA13,LAMA1,MATN2,PTEN,RERE,YWHAE
	migration of pancreatic cancer cell lines	2.92E-03	4	CDK5,FN1,PRRX1,TP53INP1
	migration of pericytes	7.70E-04	4	CCL5,CCR5,CTGF,FN1
	migration of phagocytes	1.16E-02	12	APP,CCL5,CCR5,CD58,CTGF,DDR2,FLNA,FN1,JAK1,LDLR,PTEN,TRPV1
	migration of prostate cells	4.45E-03	2	FN1,WHSC1
	migration of Purkinje cells	4.24E-05	4	CDK5,GNA13,PTEN,RERE

Supplementary Table II. Gene expression data from the 'migration of cancer cell' functional annotation relating to migration in the smooth muscle cell gene expression dataset.

Symbol	Illumina	p-value	Log Ratio	Entrez Gene ID for Human
ADAM10	ILMN_2148360	0.00749	0.32705	102
AHCY	ILMN_1657862	0.00741	-0.33416	191
CCL5	ILMN_2098126	0.00023	0.45211	6352
CSF2RA	ILMN_1661196	0.00239	0.44034	1438
CTBP2	ILMN_3250209	0.00809	0.39629	1488
CTGF	ILMN_2115125	0.00012	-0.61260	1490
CTNNB1	ILMN_1746396	0.00256	-0.36541	1499
F3	ILMN_2129572	0.00201	0.37686	2152
FN1	ILMN_1778237	0.00041	-0.45445	2335
IL11	ILMN_1788107	0.00526	0.33755	3589
LAMA5	ILMN_1773567	0.04814	-0.34166	3911
PTEN	ILMN_1880406	0.00718	-0.32989	5728
SNAI2	ILMN_1655740	0.03198	-0.34327	6591

Supplementary Table III. Gene expression data from the 'cell death and survival' functional annotation relating to survival in the endothelial cell gene expression dataset.

Categories	Diseases or Functions Annotation	p-Value	Gene Count	Molecules
Cell Death and Survival	apoptosis of follicular B lymphocytes	1.25E-03	2	BCL2A1,CD80
	cell death of B lymphocytes	1.56E-03	5	BCL11A,BCL2A1,CD80,MS4A1,VAV3
	apoptosis of pro-B lymphocytes	4.58E-03	2	BCL11A,VAV3
	apoptosis of B-2 lymphocytes	6.00E-03	1	BCL2A1
	apoptosis of B lymphocytes	7.40E-03	4	BCL11A,BCL2A1,CD80,VAV3
	apoptosis of germinal center B lymphocytes	1.79E-02	1	CD80
	loss of long-lived plasma cell	1.79E-02	1	CD80
	cell death of lymphoblastoid cell lines	2.12E-02	3	RAP1GDS1,TGIF2LX,VAV3
	apoptosis of leukocyte cell lines	2.71E-02	4	BCL2A1,IKZF3,MS4A1,PMAIP1
	apoptosis of prostate cancer cell lines	2.85E-02	4	HOXC6,IGFBP1,ILK,PMAIP1
	apoptosis of B-lymphocyte derived cell lines	4.02E-02	3	BCL2A1,MS4A1,PMAIP1
	cell viability of germ cell tumor cell lines	4.13E-02	1	PMAIP1
	apoptosis of fibrosarcoma cell lines	4.31E-02	2	BCL2A1,PMAIP1
	anoikis of breast cell lines	4.70E-02	1	ILK

Supplementary Table IV. Gene expression data from the 'cell death and survival' functional annotation relating to survival in the endothelial cell gene expression dataset.

Symbol	Illumina	p-value	Log Ratio	Entrez Gene ID for Human
BCL11A	ILMN_1752899	0.00215	0.36538	53335
BCL2A1	ILMN_1769229	0.00205	0.35285	597
CD80	ILMN_1716736	0.00333	-0.32993	941
MS4A1	ILMN_1776939	0.00339	-0.39392	931
VAV3	ILMN_2290068	0.00137	0.35903	10451

Supplemental References

1. Chien CH, Sun YM, Chang WC, Chiang-Hsieh PY, Lee TY, Tsai WC, Horng JT, Tsou AP, Huang HD. Identifying transcriptional start sites of human microrna s based on high-throughput sequencing data. *Nucleic Acids Res*. 2011;39:9345-9356
2. Xin M, Small EM, Sutherland LB, Qi X, McAnally J, Plato CF, Richardson JA, Bassel-Duby R, Olson EN. Microrna s mir-143 and mir-145 modulate cytoskeletal dynamics and responsiveness of smooth muscle cells to injury. *Genes & development*. 2009;23:2166-2178
3. Keegan A, Morecroft I, Smillie D, Hicks MN, MacLean MR. Contribution of the 5-ht(1b) receptor to hypoxia-induced pulmonary hypertension: Converging evidence using 5-ht(1b)-receptor knockout mice and the 5-ht(1b/1d)-receptor antagonist gr127935. *Circ Res*. 2001;89:1231-1239
4. Wohrley JD, Frid MG, Moiseeva EP, Orton EC, Belknap JK, Stenmark KR. Hypoxia selectively induces proliferation in a specific subpopulation of smooth muscle cells in the bovine neonatal pulmonary arterial media. *The Journal of clinical investigation*. 1995;96:273-281
5. Tuder RM, Yun JH, Bhunia A, Fijalkowska I. Hypoxia and chronic lung disease. *Journal of molecular medicine*. 2007;85:1317-1324
6. Frid MG, Brunetti JA, Burke DL, Carpenter TC, Davie NJ, Reeves JT, Roedersheimer MT, van Rooijen N, Stenmark KR. Hypoxia-induced pulmonary vascular remodeling requires recruitment of circulating mesenchymal precursors of a monocyte/macrophage lineage. *The American journal of pathology*. 2006;168:659-669
7. Neary JM, Gould DH, Garry FB, Knight AP, Dargatz DA, Holt TN. An investigation into beef calf mortality on five high-altitude ranches that selected sires with low pulmonary arterial pressures for over 20 years. *Journal of veterinary diagnostic investigation : official publication of the American Association of Veterinary Laboratory Diagnosticians, Inc*. 2013;25:210-218
8. White K, Johansen AK, Nilsen M, Ciuclan L, Wallace E, Paton L, Campbell A, Morecroft I, Loughlin L, McClure JD, Thomas M, Mair KM, MacLean MR. Activity of the estrogen-metabolizing enzyme cytochrome p450 1b1 influences the development of pulmonary arterial hypertension. *Circulation*. 2012;126:1087-1098
9. Stiebellehner L, Frid MG, Reeves JT, Low RB, Gnanasekharan M, Stenmark KR. Bovine distal pulmonary arterial media is composed of a uniform population of well-differentiated smooth muscle cells with low proliferative capabilities. *American journal of physiology. Lung cellular and molecular physiology*. 2003;285:L819-828
10. Caruso P, Dempsie Y, Stevens HC, McDonald RA, Long L, Lu R, White K, Mair KM, McClure JD, Southwood M, Upton P, Xin M, van Rooij E, Olson EN, Morrell NW, MacLean MR, Baker AH. A role for mir-145 in pulmonary arterial hypertension: Evidence from mouse models and patient samples. *Circ Res*. 2012;111:290-300

11. Ritchie ME, Phipson B, Wu D, Hu Y, Law CW, Shi W, Smyth GK. Limma powers differential expression analyses for rna-sequencing and microarray studies. *Nucleic acids research*. 2015;43:e47
12. Louch WE, Sheehan KA, Wolska BM. Methods in cardiomyocyte isolation, culture, and gene transfer. *Journal of molecular and cellular cardiology*. 2011;51:288-298
13. Meloche J, Pflieger A, Vaillancourt M, Paulin R, Potus F, Zervopoulos S, Graydon C, Courboulin A, Breuils-Bonnet S, Tremblay E, Couture C, Michelakis ED, Provencher S, Bonnet S. Role for DNA damage signaling in pulmonary arterial hypertension. *Circulation*. 2014;129:786-797
14. Rodrigue A, Lafrance M, Gauthier MC, McDonald D, Hendzel M, West SC, Jasin M, Masson JY. Interplay between human DNA repair proteins at a unique double-strand break in vivo. *EMBO J*. 2006;25:222-231